

# Sulfur Chemistry in the Atmospheres of Warm and Hot Jupiters

Richard Hobbs,<sup>1</sup>★ Paul B. Rimmer<sup>2,3,4</sup> Oliver Shorttle,<sup>1,2</sup> and Nikku Madhusudhan<sup>1</sup>

<sup>1</sup>*Institute of Astronomy, University of Cambridge, Cambridge, CB3 0HA, UK*

<sup>2</sup>*Cambridge Earth Sciences, University of Cambridge, Cambridge CB2 3EQ, UK*

<sup>3</sup>*MRC Laboratory of Molecular Biology, Cambridge, CB2 0QH, UK*

<sup>4</sup>*Cavendish Astrophysics, University of Cambridge, Cambridge, CB3 0HE, UK*

Accepted XXX. Received YYY; in original form ZZZ

## ABSTRACT

We present and validate a new network of atmospheric thermo-chemical and photo-chemical sulfur reactions. We use a 1-D chemical kinetics model to investigate these reactions as part of a broader HCNO chemical network in a series of hot and warm Jupiters. We find that temperatures approaching 1400 K are favourable for the production of H<sub>2</sub>S and HS around 10<sup>-3</sup> bar, the atmospheric level where detection by transit spectroscopy may be possible, leading to mixing ratios of around 10<sup>-6</sup>. At lower temperatures, down to 1000 K, the abundance of S<sub>2</sub> can be up to a mixing ratio of 10<sup>-5</sup> at the same pressure, at the expense of H<sub>2</sub>S and HS, which are depleted down to a mixing ratio of 10<sup>-6</sup>. We also investigate how the inclusion of sulfur can manifest in an atmosphere indirectly, by its effect on the abundance of non-sulfur-bearing species. We find that in a model of the atmosphere of HD 209458 b, the inclusion of sulfur can lower the abundance of NH<sub>3</sub>, CH<sub>4</sub> and HCN by up to two orders of magnitude around 10<sup>-3</sup> bar. In the atmosphere of the warm Jupiter 51 Eri b, we additionally find the inclusion of sulphur depletes the peak abundance of CO<sub>2</sub> by a factor of five, qualitatively consistent with prior models. We note that many of the reactions used in the network have poorly determined rates, especially at higher temperatures. To obtain a truly accurate idea of the impact of sulfur chemistry in hot and warm Jupiter atmospheres, new measurements of these reaction rates must take place.

**Key words:** planets and satellites: gaseous planets – planets and satellites: atmospheres – planets and satellites: composition – planets and satellites: individual (HD 209458b, 51 Eri b)

## 1 INTRODUCTION

Sulfur chemistry is known to play an important role in the atmospheric chemistry of planets in our solar system. In the past, it may have lead to the first Snowball Earth event (Macdonald & Wordsworth 2017), and sulfur isotope ratios can be used as a tracer of Earth’s Great Oxidation Event (Hodgskiss et al. 2019). Sulfur photochemistry is thought to influence the production of hazes and clouds in the upper atmospheres of solar system planets such as Earth (Malin 1997), Venus (Zhang et al. 2012; Titov et al. 2018), Jupiter (Moses et al. 1995) and the moon Io (Irwin 1999). Similar hazes, expected to appear in the atmospheres of exoplanets (He et al. 2020), would greatly affect their observed spectra. This would limit our ability to examine their atmosphere, and make assessments of their habitability challenging (Gao et al. 2017).

Sulfur has also recently been of interest in the field of Jupiter-like exoplanets. A tentative detection of the mercapto radical, HS, in the atmosphere of the hot Jupiter WASP-121 b has been made (Evans et al. 2018). However, it is still uncertain whether HS or another molecule is responsible for the absorption feature seen. The warm

Jupiter 51 Eri b has also been an excellent example of the importance of sulfur chemistry. Two groups have produced models of 51 Eri b’s atmosphere, one study did not include sulfur chemistry (Moses et al. 2016) and the other did include sulfur chemistry (Zahnle et al. 2016). Significant differences were found between the two models, in particular in the modelled abundance of CO<sub>2</sub>, but it was unknown whether this was due to sulfur chemistry or other differences in the models. Thus it is important to include sulfur chemistry in models of exoplanets, both terrestrial and gas-giant, to obtain an accurate picture of their atmospheric composition.

However, very few models exist that include sulfur chemistry for exoplanet atmospheres. Hu et al. (2013) investigate the photochemistry of H<sub>2</sub>S and SO<sub>2</sub> in terrestrial planet and conclude that their direct detection is unlikely due to rapid photochemical conversion to elemental sulfur and sulfuric acid. Visscher et al. (2006) examine thermo-chemical sulfur chemistry for the hot, deep atmospheres of sub-stellar objects and find H<sub>2</sub>S to be the dominant sulfur bearing gas. However, due to the high temperatures and pressures of the atmospheres they are studying, disequilibrium effects such as diffusion or photochemistry are not considered. Zahnle et al. (2009) investigate whether sulfur photochemistry could explain the hot stratospheres of hot Jupiters, and find that UV absorption of

★ E-mail: rh567@cam.ac.uk

HS and S<sub>2</sub> may provide an explanation. Zahnle et al. (2016) also investigate whether sulfur could form photochemical hazes in the atmosphere of 51 Eri b, and under what conditions they could be formed. They find that sulfur clouds should appear on many planets where UV irradiation is weak.

We need models to be able to investigate the effects of sulfur on exoplanet atmospheres. One way of modelling the atmosphere of planets is through the use of chemical kinetics models. These exist in the form of 1-D (e.g., Moses et al. 2011; Venot et al. 2012; Rimmer & Helling 2016; Tsai et al. 2017), 2-D (e.g., Agúndez et al. 2014) and 3-D (e.g. Drummond et al. 2018) models. The 1-D models take a network of possible chemical reactions within an atmosphere and a temperature profile of the atmosphere to produce abundance profiles of chemical species. These models are frequently combined with prescriptions for diffusion and include a UV flux applied to the top of the model, to allow a full disequilibrium model to be created. Atmospheric models are obtained by computing these models until they reach a converged steady-state condition.

Throughout the last few decades, chemical models of exoplanetary atmospheres have grown more detailed and complex. What had begun as equilibrium models containing limited molecular species made of only a few elements in small chemical networks (e.g., Lodders & Fegley 2002; Liang et al. 2003; Zahnle et al. 2009) have evolved into large photo-kinetic models containing hundreds of molecular species made of many elements in chemical networks with thousands of reactions (Moses et al. 2011; Venot et al. 2012; Rimmer & Helling 2016). The focus of this work is to continue this evolution. We do so by introducing a new element, sulfur, to the model and to the network, both described in our previous paper (Hobbs et al. 2019). In this way we can produce a tested and validated network of sulfur chemistry. In this work we apply the network to hot and warm Jupiters. By doing so, we can investigate the importance of sulfur in the atmospheres of exoplanets in both the context of sulfur itself and the way it impacts carbon and oxygen chemistry.

We begin with a brief overview of the model we're using. In Section 3 we validate our network for pure thermo-chemical equilibrium and compare our model against the sulfur model of Zahnle et al. (2009). Section 4 contains our analysis of the sulfur chemistry occurring in the atmospheres of hot Jupiters, and shows which pathways in our network lead to such chemistry occurring. In Section 5, we examine how sulfur can affect the chemistry of other, non-sulfur species in both warm and hot Jupiters. We discuss our findings and review what we have discovered in Section 6.

## 2 MODEL DETAILS

To investigate sulfur chemistry in the atmospheres of hot Jupiters, we chose to use LEVI, a one-dimensional photo-kinetics code, originally described in Hobbs et al. (2019). This code was previously developed to model carbon, oxygen and nitrogen chemistry in hot Jupiter atmospheres. It was validated against several other photo-chemical models of hot Jupiters.

In this work, LEVI, is being used to model the atmospheres of Jupiter-like planets. It does so via calculations of:

- The interactions between chemical species
- The effects of vertical mixing due to eddy-diffusion molecular diffusion and thermal diffusion
- Photochemical dissociation due to an incoming UV flux.

And uses the input parameters of:

- The pressure-temperature (P-T) profile of the atmosphere
- The eddy-diffusion ( $K_{zz}$ ) profile of the atmosphere
- The profiles of the UV stellar spectrum
- The metallicity of the atmosphere
- The gravity of the planet.

It uses the assumptions of:

- hydrostatic equilibrium
- The atmosphere being an ideal gas
- The atmosphere is small compared to the planet, such that gravity is constant throughout the atmospheric range being modelled.

By combining all of these factors, abundance profiles of the atmosphere are computed.

As is typical for codes of this type, LEVI finds steady-state solutions for species in the atmosphere by solving the coupled one-dimensional continuity equation:

$$\frac{\partial n_i}{\partial t} = \mathcal{P}_i - \mathcal{L}_i - \frac{\partial \Phi_i}{\partial z}, \quad (1)$$

where  $n_i$  ( $\text{m}^{-3}$ ) is the number density of species  $i$ , with  $i = 1, \dots, N_i$ , with  $N_i$  being the total number of species.  $\mathcal{P}_i$  ( $\text{m}^{-3} \text{s}^{-1}$ ) and  $\mathcal{L}_i$  ( $\text{m}^{-3} \text{s}^{-1}$ ) are the production and loss rates of the species  $i$ .  $\partial t$  (s) and  $\partial z$  (m) are the infinitesimal time step and altitude step respectively.  $\Phi_i$  ( $\text{m}^{-2} \text{s}^{-1}$ ) is the upward vertical flux of the species, given by,

$$\Phi_i = -(K_{zz} + D_i)n_t \frac{\partial X_i}{\partial z} + D_i n_i \left( \frac{1}{H_0} - \frac{1}{H} - \frac{\alpha_{T,i}}{T} \frac{dT}{dz} \right), \quad (2)$$

where  $X_i$  and  $n_t$  ( $\text{m}^{-3}$ ) are the mixing ratio and total number density of molecules such that  $n_i = X_i n_t$ . The eddy-diffusion coefficient,  $K_{zz}$  ( $\text{m}^2 \text{s}^{-1}$ ), approximates the rate of vertical transport and  $D_i$  ( $\text{m}^2 \text{s}^{-1}$ ) is the molecular diffusion coefficient of species  $i$ .  $H_0$  (m) is the mean scale height,  $H$  (m) is the molecular scale height,  $T$  (K) is the temperature, and  $\alpha_{T,i}$  is the thermal diffusion factor. For the full explanation of how we determine each of these parameters, and solved the equations, refer to Hobbs et al. (2019).

Previously, we used a subset of the Stand2019 network. This was the Stand2015 network first developed in Rimmer & Helling (2016) plus the additional reactions from Rimmer & Rugheimer (2019). We limited it to only reactions with neutral species containing hydrogen, carbon, nitrogen and oxygen, in conjunction with LEVI to model hot Jupiter atmospheres. As part of this work we have developed a new addition to this network, comprised of 185 reactions and 30 species that include the element sulfur. Our sulfur species include molecules that contain up to 2 H, 3 C, 3 O and 2 S, except for the allotropes of sulfur that include up to S<sub>8</sub>. These species are tabulated in Table 1. These reactions were mainly drawn from the NIST chemical kinetics database<sup>1</sup>, with the full tabulation of both reactions and sources available in the table of Appendix A.

We attempted to apply a sensible selection criterion when choosing which sources of the rate constants to use for each reaction. Where possible, we selected rate constants that had been measured experimentally, rather than theoretically. This network was intended to be able to apply to hot Jupiters, whose temperatures can reach several thousand Kelvin. As such, we aimed to pick rate constants that had been measured over a range of temperatures, ideally to temperatures that are realistic for a hot Jupiter, i.e.,

<sup>1</sup> <https://kinetics.nist.gov/kinetics/>

**Table 1.** Chemical names of the sulfur species used in the network

Species	Chemical Name
S	Sulfur
S <sub>2</sub>	Disulfur
S <sub>3</sub>	Trisulfur
S <sub>4</sub>	Tetrasulfur
S <sub>5</sub>	Pentasulfur
S <sub>6</sub>	Hexasulfur
S <sub>7</sub>	Heptasulfur
S <sub>8</sub>	Octasulfur
HS	Mercapto Radical
H <sub>2</sub> S	Hydrogen Sulfide
H <sub>2</sub> S <sub>2</sub>	Hydrogen Disulfide
CS	Carbon Sulfide
CS <sub>2</sub>	Carbon Disulfide
CS <sub>2</sub> OH	Thioxomethyl Radical
HCS	Thioformyl Radical
OCS	Carbonyl Sulfide
H <sub>2</sub> CS	Thioformaldehyde
H <sub>2</sub> C <sub>3</sub> S	Tricarbon Monosulfide
CH <sub>3</sub> SH	Mercaptomethane
HSNO	Thionylimide
SO	Sulfur Monoxide
SO <sub>2</sub>	Sulfur Dioxide
SO <sub>3</sub>	Sulfur Trioxide
S <sub>2</sub> O	Disulfur Monoxide
HSO	Sulfenate
HSO <sub>2</sub>	Sulfinate
HSO <sub>3</sub>	Bisulfite
HOSO	Hydroperoxysulfanyl
HSOO	HSOO

2000 K. Unfortunately, many reactions have only been measured at room temperature, resulting in currently unavoidable limitations to the accuracy of these reaction rates. Finally, we in general picked the more recently measured rate constants, although many have not had new measurements in many decades. In some cases, the rates of both the forward and reverse reaction were available. In these cases, we tried to pick the rates for the reaction without an energy barrier, and used thermodynamic reversal to obtain the rates for the reverse reaction. We took the estimated rates of sulfur allotrope polymerisation from Moses et al. (2002) and several carbon monosulphide, CS, reactions from the KIDA database (Wakelam et al. 2012)<sup>2</sup>. All of these reactions are thermodynamically reversed using the NASA9 polynomials from Burcat<sup>3</sup>. We also include the photodissociation cross-sections for 17 reactions involving eleven sulfur species: S<sub>2</sub>, S<sub>3</sub>, S<sub>4</sub>, H<sub>2</sub>S, SO, SO<sub>2</sub>, SO<sub>3</sub>, S<sub>2</sub>O, OCS, CS<sub>2</sub> and CH<sub>3</sub>SH. The photo-dissociation cross-section,  $\Sigma_{i \rightarrow j}$  (m<sup>2</sup>) is equal to  $\sigma_{a,i} \times q_{a,i \rightarrow j}$ , where  $\sigma_{a,i}$  (m<sup>2</sup>) is the absorption cross-section and  $q_{a,i \rightarrow j}$  is the quantum yield. The wavelengths  $i = 1 \text{ \AA}$  and  $j = 10000 \text{ \AA}$  are the range over which we use these cross-sections. The cross-sections for H<sub>2</sub>S, SO, SO<sub>2</sub>, OCS, CS<sub>2</sub> and CH<sub>3</sub>SH were taken from PhIDrates<sup>4</sup>, the cross-sections for S<sub>3</sub>, S<sub>4</sub> and S<sub>2</sub> from the MPI-Mainz-UV-VIS Spectral Atlas of Gaseous Molecules<sup>5</sup> and the cross-section for S<sub>2</sub> from the Leiden database (Heays et al. 2017).

Here we define which parameters are consistent throughout all models, and what changes are applied to specific models. In all of our models we set the boundary conditions at the top and bottom of

the atmosphere to be zero-flux, such that there is no interaction with the atmosphere outside of our model. Additionally, when we apply a UV flux to our atmospheres, we choose a mean zenith angle of 57.3° (Zahnle et al. 2008; Hu et al. 2012), and we model the planet as if its day-side is always facing the star it orbits, i.e. it's tidally locked. Most of our models use a solar metallicity, with values from Asplund et al. (2009). This gives an elemental ratio, as a fraction of the total number of molecules, of:  $X_{\text{H}_2} = 0.5 \times X_{\text{H}} = 0.8535$ ,  $X_{\text{He}} = 0.145$ ,  $X_{\text{C}} = 4.584 \times 10^{-4}$ ,  $X_{\text{O}} = 8.359 \times 10^{-4}$ ,  $X_{\text{N}} = 1.154 \times 10^{-4}$ ,  $X_{\text{S}} = 2.250 \times 10^{-5}$ . When we alter the metallicity, we proportionally change the amount of C, O, N and S in the atmosphere. He is kept constant, and H<sub>2</sub> is altered such that the ratios sum to unity.

There are also parameters that vary between each model. This includes: the pressure-temperature (P-T) profile, the gravity of the planet, the eddy-diffusion profile applied to the model and the spectral irradiance applied to the top of the atmosphere. An overview of these differences can be seen in Table 2.

### 3 VALIDATION OF THE NETWORK

In this section we test our model by applying it to the atmospheres of several hot Jupiters. We compare the thermochemistry of our model to an analytical equilibrium solver, FastChem (Stock et al. 2018). We also compare and contrast our complete model to a previous sulfur model produced by Zahnle et al. (2009).

#### 3.1 Equilibrium Comparison

As a first step of validating our new sulfur network, we chose to consider our results when considering only thermochemistry, with no disequilibrium chemistry. We compare to the analytical equilibrium output of FastChem, a chemical equilibrium solver produced by Stock et al. (2018). In this comparison, we chose to compare a hot Jupiter atmosphere model with an isothermal temperature of 1400 K. The results of this are shown in Figure 1, where we display only the important sulfur species for comparison. We have a near perfect match compared to the analytic output for every species except for HS, which we slightly under-produce, and OCS, which we slightly over-produce.

We expect the causes for these slight dissimilarities to be due to differences in the thermochemical constants we use to reverse our reaction rates. We use the NASA9 polynomials from Burcat<sup>6</sup> to calculate our Gibbs free energy, while Stock et al. (2018) drew theirs from thermochemical databases, e.g., Chase (1998).

Overall, it can be seen that the thermochemistry of our sulfur network is an excellent match to the analytical solution of FastChem. The slight differences seen between the two models are not large enough to significantly impact the chemistry occurring in the atmosphere. Additionally, the difference would not be detectable to observations.

#### 3.2 Comparison with a previous sulfur network

The network from Zahnle et al. (2009) was originally produced to examine the effects of sulfur photochemistry on stratospheric chemistry and heating in hot Jupiters. We make comparisons between our new network and the model of Zahnle et al. (2009) for two hot Jupiter models, shown in Figures 2 and 3.

<sup>2</sup> <http://kida.astrophy.u-bordeaux.fr/>

<sup>3</sup> <http://garfield.chem.elte.hu/Burcat/burcat.html>

<sup>4</sup> <https://phidrates.space.swri.edu/>

<sup>5</sup> [www.uv-vis-spectral-atlas-mainz.org](http://www.uv-vis-spectral-atlas-mainz.org)

<sup>6</sup> <http://garfield.chem.elte.hu/Burcat/burcat.html>

**Table 2.** Model Parameters

Case	Analogue Planet	$T$ -profile K	Gravity $\text{cm s}^{-2}$	$K_{zz}$ -profile $\text{cm}^2 \text{s}^{-1}$	Metallicity	TOA Spectral Irradiance $\text{photons cm}^{-2} \text{s}^{-1} \text{\AA}^{-1}$
Figure 1	Hot Jupiter	1400	1000	None	Solar	None
Figure 2	Hot Jupiter	1400	1000	$10^7$	$[M/H] = 0.7$	$1000\times$ Solar
Figure 3	WASP-121 b	<a href="#">Evans et al. (2018)</a>	875	$10^9$	$[M/H] = 1.3$	$5300\times$ Solar
Figure 4	Hot Jupiter	Multiple	1000	None	Solar	None
Figure 5	Hot Jupiter	Multiple	1000	$10^9$	Solar	$10\times$ Solar
Figure 6	Hot Jupiter	1200	1000	Multiple	Solar	$10\times$ Solar
Figure 7	Hot Jupiter	1200	1000	$10^9$	Solar	Multiple
Figure 8	HD 209458 b	<a href="#">Hobbs et al. (2019)</a>	936	<a href="#">Hobbs et al. (2019)</a>	Solar	$800\times$ Solar
Figure 9	51 Eri b	<a href="#">Moses et al. (2016)</a>	3200	$10^7$	Solar	<a href="#">Moses et al. (2016)</a>

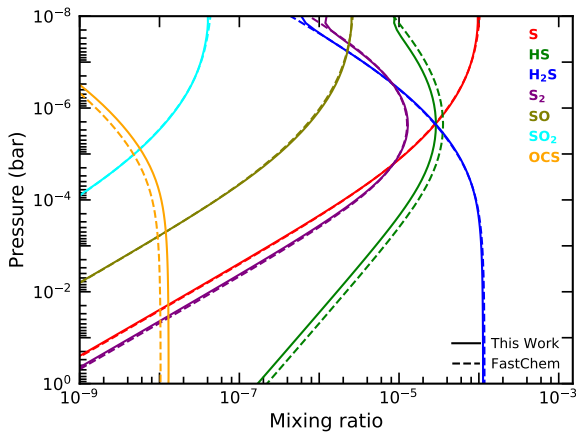


**Figure 1.** The abundances of significant sulfur bearing species for a purely thermochemical chemistry calculation, taking place in a hot Jupiter atmosphere model that is isothermal at 1400 K, has a gravity of  $10 \text{ ms}^{-2}$  and a metallicity  $5\times$  solar. It has no diffusion or UV spectrum applied to the atmosphere. The solid lines are the output of the model being discussed in this work, while the dashed lines are from the analytical equilibrium solver of FastChem ([Stock et al. 2018](#)).

In Figure 2, the comparison is made for a hot Jupiter model with an isothermal atmosphere at 1400 K, a  $K_{zz} = 10^7 \text{ cm}^2 \text{ s}^{-1}$ , insolated  $1000\times$  more strongly than Earth and with a metallicity that is  $5\times$  solar. In this figure, there are two main regimes that should be examined. The first is deep in the atmosphere where the pressure is greater than  $10^{-3}$  bar. The chemistry at this level is mainly determined by the thermochemistry, due to the high temperatures and pressures. The second chemical regime is higher in the atmosphere, where the pressure is less than  $10^{-3}$  bar, and where disequilibrium effects such as diffusion and photochemistry are expected to dominate.

Figure 2 shows that the outcome of the sulfur chemistry of our network in the deeper atmosphere is significantly different than that of [Zahnle et al. \(2009\)](#). In our model, the abundances of HS,  $\text{S}_2$ , S, SO and  $\text{SO}_2$  are all at least two orders of magnitude less than that seen in [Zahnle et al. \(2009\)](#). This result is not unexpected, since the thermochemistry of [Zahnle et al. \(2009\)](#) was known to have systematic discrepancies (K. Zahnle personal communication 2020). These discrepancies were corrected in a later work ([Evans et al. 2018](#)). However, we expect thermochemical processes to dominate at this pressure, and, as seen in section 3.1 and figure 1, there is an excellent match between the output of our model and the thermochemical equilibrium results from FastChem. For the non-sulfur

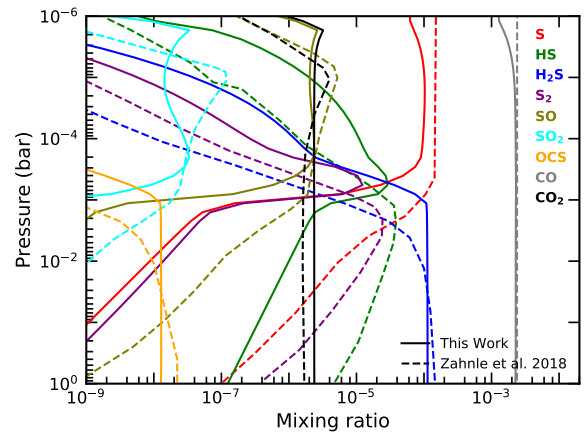


**Figure 2.** A comparison between our network (solid lines) and one presented in [Zahnle et al. \(2009\)](#) (dashed lines) for a hot Jupiter model. This atmosphere is isothermal with a temperature of 1400 K, a gravity of  $10 \text{ ms}^{-2}$ ,  $K_{zz} = 10^7 \text{ cm}^2 \text{ s}^{-1}$ , with a metallicity  $5\times$  solar and insolated  $1000\times$  stronger than Earth.

bearing species, there is a good match between our models. Thus, we have reason to believe that the sulfur thermochemistry in our model is accurate.

Higher in the atmosphere, our model matches more closely with that of [Zahnle et al. \(2009\)](#). The abundance of nearly every species is within a factor of five between the two models. The differences that are present are likely caused by our choices for the photochemical cross-sections compared to [Zahnle et al. \(2009\)](#), but overall the abundance profiles are very similar.

In Figure 3 we show our model for the hot Jupiter WASP-121 b, and compare to the abundance profile presented in [Evans et al. \(2018\)](#) and produced by the model of [Zahnle et al. \(2009\)](#). This hot Jupiter has a metallicity of  $20\times$  solar and constant  $K_{zz} = 10^9 \text{ cm}^2 \text{ s}^{-1}$ . The model in [Evans et al. \(2018\)](#) used an F6V host star, whereas here we use a solar host star, with its spectrum scaled as if it were the size and temperature of WASP-121. Just as in Figure 2, we can broadly split the atmosphere into two sections, pressures greater than  $10^{-3}$  bar where thermochemical effects are expected to be more important and pressures less than  $10^{-3}$  bar where we expect to see photochemistry dominating.

In the deep atmosphere, Figure 3 shows that our model has close agreement with the model of [Evans et al. \(2018\)](#), with a difference in predicted abundances of less than 50% between the models. We observe a systematic under-abundance of S-bearing species in our model compared with that of [Evans et al. \(2018\)](#), as the

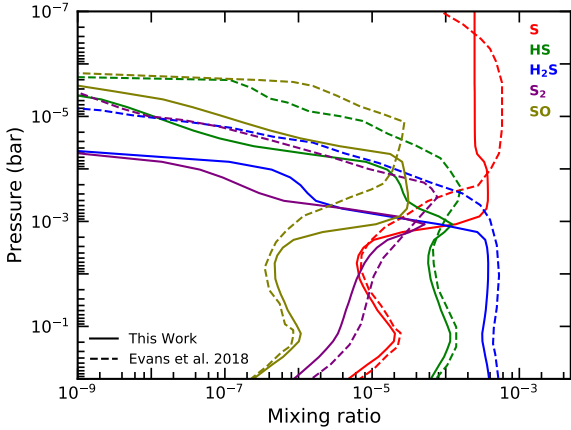


**Figure 3.** A comparison between our network (solid lines) and one presented in [Evans et al. \(2018\)](#), but created by the code of [Zahnle et al. \(2009\)](#) (dashed lines) for a model of WASP-121 b. The P-T profile for this model is taken from [Evans et al. \(2018\)](#), with constant  $K_{zz} = 10^9 \text{ cm}^2 \text{ s}^{-1}$ , a gravity of  $8.75 \text{ ms}^{-2}$  and a metallicity  $20\times$  solar. The UV spectrum applied to the top of the atmosphere is  $5300\times$  Earth’s insolation.

non-S species match closely. This likely reflects a slightly different atmospheric composition being used. More significant differences can be seen in the upper atmosphere, with most of the displayed species varying by several orders of magnitude. We expect this to be primarily due to the difference in the stellar spectrum being applied to this atmosphere. It can be seen in [Figure 3](#) that the general shape of the abundance profiles are very similar, except that our model predicts photochemistry to begin deeper into the atmosphere, a result consistent with the stronger UV spectrum of a G2V star penetrating further. The only other major difference seen in this figure is the profile of S in the upper atmosphere. We believe it to be as a result of differences in how the models treat molecular diffusion.

The network is also being used in [Rimmer et al. \(2021\)](#) to model sulfur chemistry on Venus. The model in that work produces results very similar to the observations of Venus’s atmosphere, suggesting that the network is valid down to temperatures in the middle atmosphere of Venus; as low as 200 K.

In conclusion, after comparing our new sulfur model against the sulfur model from [Zahnle et al. \(2009\)](#) and [Evans et al. \(2018\)](#), we see both similarities and differences in the way we treated thermochemistry and photochemistry. We are confident in the accuracy of our thermochemistry after comparisons with the analytical chemical equilibrium solver in [Section 3.1](#). Also, our thermochemical results are very similar to those seen in [Evans et al. \(2018\)](#). Comparing photochemistry is more difficult, but overall the structure of the abundance profiles suggests the photochemistry between this work and [Zahnle et al. \(2009\)](#) is similar. The discrepancies that can be seen are likely due to differences in UV cross-sections and stellar spectrum.

## 4 SULFUR IN HOT JUPITERS

In this section, we investigate sulfur chemistry in the atmosphere of hot Jupiters. We identify the major sulfur species throughout the atmosphere, and note how and why the abundance of these species

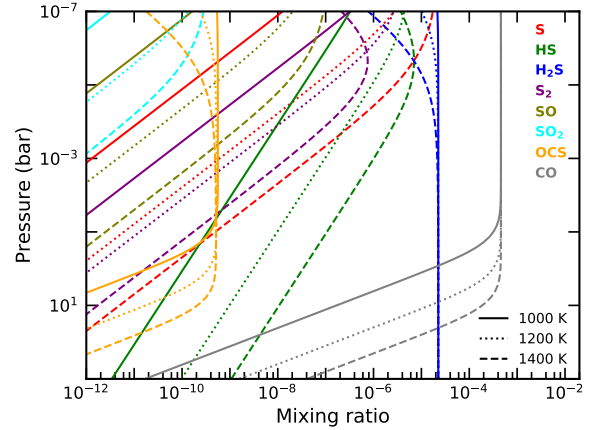


**Figure 4.** Sulfur chemistry in three isothermal (1000K, 1200K and 1400K) hot Jupiter atmospheres in local thermodynamic equilibrium. This atmosphere has a solar metallicity and a gravity of  $10 \text{ ms}^{-2}$ . It has no diffusion or UV spectrum applied to it.

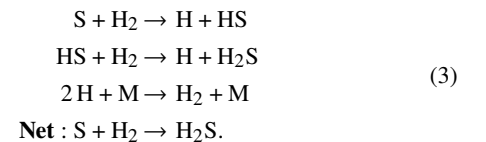
change. We consider this change in relation to both the planet’s temperature and other properties such as diffusion.

### 4.1 Local Thermodynamic Equilibrium

To begin with, we investigate the simplest scenario for sulfur chemistry in hot Jupiters: An isothermal atmosphere model that is purely in local thermodynamic equilibrium, without any form of diffusion or photochemistry.

In [Figure 4](#) we show comparisons of three isothermal atmospheres in chemical equilibrium. The isothermal temperatures of these atmospheres are 1000 K (Solid), 1200 K (Dotted) and 1400 K (Dashed). All three have a solar metallicity and a gravity of  $10 \text{ ms}^{-2}$ . We plot carbon monoxide, CO, and sulfur bearing species that have a mixing ratio greater than  $10^{-10}$  at any point in the atmosphere. In this manner we can show the full scope of sulfur chemistry throughout the entire atmosphere.

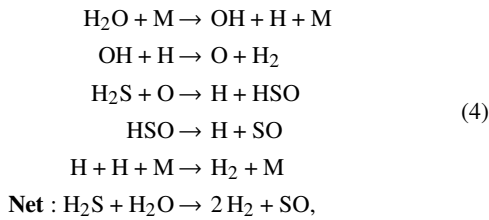
The first point of note is the preference of sulfur to form  $\text{H}_2\text{S}$ . At all temperatures shown,  $\text{H}_2\text{S}$  is the primary carrier of sulfur throughout the majority of the atmosphere, with an abundance of  $2 \times 10^{-5}$  for most of the deep atmosphere. It is only at low pressures along the hottest isotherms where this changes, with the primary sulfur carrier becoming atomic S. The reactions that set these abundances are



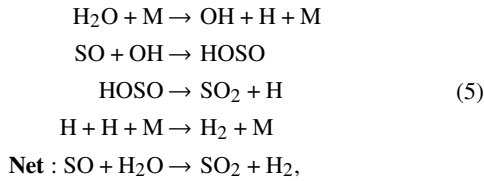
High temperatures favour the left hand side of this net equation, preferring to dissociate  $\text{H}_2\text{S}$  to its constituent  $\text{H}_2$  and S. In comparison, high pressures favour the formation of  $\text{H}_2\text{S}$  from  $\text{H}_2$  and S. This is why S becomes the most abundant sulfur molecule only at very low pressures along the high temperature isotherms. The mercapto radical, HS, is also of interest, as it acts as an intermediary between S and  $\text{H}_2\text{S}$ . HS forms a steady pool that quickly reacts to either S or  $\text{H}_2\text{S}$ , depending on which is more thermodynamically favoured. Generally, the higher temperature atmospheres favour HS. In all

three models, lower pressure increases the abundance of HS. This is unsurprising since, as previously mentioned, the higher temperature and lower pressure favour the dissociation of the large pool of H<sub>2</sub>S, creating more HS as a result. Although, at the very top of the atmosphere, above 10<sup>-7</sup> bar, this changes. Here, the abundance of HS in the 1400 K atmosphere decreases with pressure and drops below the abundance of HS in the 1200 K atmosphere. This result arises from atomic S now being the primary sulfur carrier, since its production is favoured by both temperature and pressure. With the majority of sulfur now being in S, the equilibrium abundance of HS decreases.

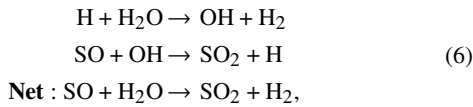
Both sulfur oxides, SO and SO<sub>2</sub>, follow similar patterns throughout the atmosphere. They increase in abundance with decreasing pressure, and are more abundant in higher temperature atmospheres. The production pathway for SO is



and for SO<sub>2</sub> is



for the deep atmosphere, or more directly



for the upper atmosphere.

The sulfur molecules HSO and HOSO referenced in these pathways are not shown in Figure 4 due to their very low abundance. The production of both SO and SO<sub>2</sub> starts with the destruction of H<sub>2</sub>S by an oxygen radical, O. This produces the short lived species HSO that quickly dissociates into SO. SO subsequently reacts with the hydroxyl radical, OH. At pressures greater than 10<sup>-1</sup> bar, this reaction forms the very short lived species HOSO, that then dissociates into SO<sub>2</sub>. At pressures less than 10<sup>-1</sup> bar, SO and OH react directly to form SO<sub>2</sub>. The production of SO is significantly faster than the reaction rate of SO with OH. As a result, the equilibrium abundance of SO is much larger than that of SO<sub>2</sub>. Near the top of the atmosphere, above 10<sup>-6</sup> bar in the 1400 K isothermal atmosphere, the abundances of SO and SO<sub>2</sub> stop increasing with decreasing pressure. This happens due to the H<sub>2</sub>S abundance dropping. It is now no longer as available to start the production pathway of SO and SO<sub>2</sub>.

The pathway producing the sulfur molecule OCS is

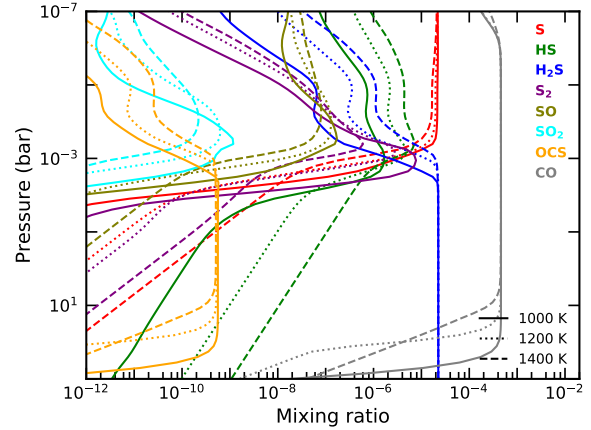
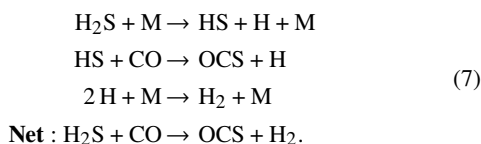
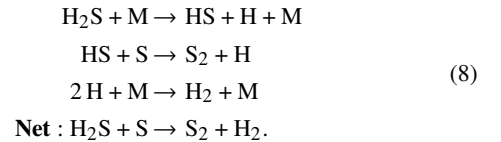


**Figure 5.** Sulfur chemistry in three isothermal (1000K, 1200K and 1400K) hot Jupiter atmospheres in steady-state. This atmosphere has a solar metallicity, a gravity of 10 ms<sup>-2</sup>, constant  $K_{zz} = 10^9$  cm<sup>2</sup>s<sup>-1</sup> and a UV flux 10× Earth’s.

In the deep atmosphere, below 10<sup>-1</sup> bar, the abundance of OCS is controlled by the abundance of CO. Above this pressure, there is a zone for which both H<sub>2</sub>S and CO have a constant abundance. This leads OCS to stay at a constant abundance at these pressures. Above 10<sup>-4</sup> bar for the 1400 K atmosphere, and 10<sup>-6</sup> bar for the 1200 K atmosphere, the drop in the abundance of H<sub>2</sub>S results in the mixing ratio of OCS decreasing at a similar rate.

The allotrope of sulfur, S<sub>2</sub>, is produced by the pathway



Thus the abundance of S<sub>2</sub> is controlled by the abundance of S and HS (and therefore H<sub>2</sub>S). This results in a general increase of abundance as pressure decreases. The exception is for the case of the 1400 K isotherm, where the drop in abundance of H<sub>2</sub>S and HS above 10<sup>-6</sup> bar leads to a decrease in the mixing ratio of S<sub>2</sub>.

## 4.2 Disequilibrium

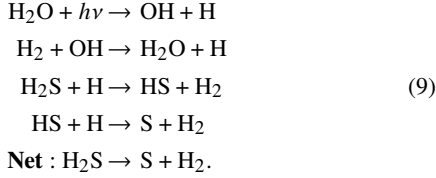
The atmosphere of most planets are not in chemical equilibrium at low pressure (< 10<sup>-3</sup> bar). Therefore it is important to consider how the disequilibrium effects of diffusion and photochemistry can impact the expected sulfur chemistry in a planets atmosphere.

In Figure 5 we show the same three isothermal atmospheres as in the previous section: Isotherms of 1000 K (Solid), 1200 K (Dotted) and 1400 K (Dashed). Once again, all three have a solar metallicity and a gravity of 10 ms<sup>-2</sup>. All of these atmospheres now have a constant eddy diffusion  $K_{zz} = 10^9$  cm<sup>2</sup>s<sup>-1</sup>. They also have a UV spectrum applied to the top of the atmosphere of 10× Earth’s received solar flux.

In the deep atmosphere, below about 10<sup>-1</sup> bar, the abundances are near identical to the equilibrium results presented in the previous section. At this depth, the high pressure ensures that the reaction rates are fast enough that the disequilibrium effects of diffusion and photo-dissociation does not have a significant impact on the chemistry previously presented.

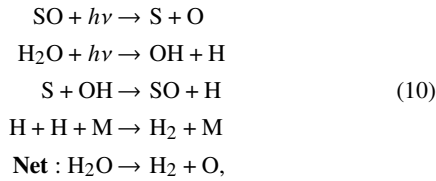
Higher in the atmosphere, above  $10^{-3}$  bar, we start to see the significance of disequilibrium chemistry. Many of the sulfur molecules are susceptible to photo-dissociation.

Once again  $\text{H}_2\text{S}$  is of particular note. At  $10^{-3}$  bar it is rapidly dissociated by free H radicals that are produced by photolysis, and then diffuse down from higher in the atmosphere

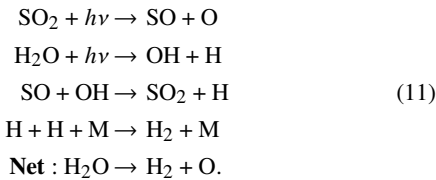


This effect occurs at all temperatures. Although, in the colder models, we see the abundance of  $\text{H}_2\text{S}$  driven much further away from its equilibrium value, by more than two orders of magnitude, compared to the hotter models. This is because of the longer chemical timescales at lower temperatures, which slows the recombination reactions. Overall, the rapid destruction of  $\text{H}_2\text{S}$  allows for the abstraction of sulfur into atomic S very efficiently. This results in S being the primary sulfur molecule at all temperatures and pressures above  $10^{-3}$  bar.

The production of a large available pool of S has knock-on effects for the abundance of SO and  $\text{SO}_2$ . Above  $10^{-3}$  bar the abundance of SO is controlled by the reaction chain of



and  $\text{SO}_2$  by a very similar loop



Overall, both these reaction pathways act as a dissipative cycle that increases the abundance of atomic O in the atmosphere, while preventing SO and  $\text{SO}_2$  from being permanently dissociated. The abundances of both SO and  $\text{SO}_2$  are primarily determined by the amount of atomic S in the atmosphere. As a result the abundances of SO and  $\text{SO}_2$  are nearly temperature independent throughout the upper atmosphere. SO reaches abundances around  $10^{-7}$ , while  $\text{SO}_2$  is never greater than  $10^{-9}$ .

$\text{S}_2$  is significantly affected by the introduction of disequilibrium chemistry. The large increase in both HS and S around  $10^{-3}$  bar greatly boosts its production through the reaction



This is particularly prominent in the lower temperature isotherms. In the 1000 K atmosphere, the abundance of  $\text{S}_2$  reaches nearly  $10^{-5}$  (compared to only  $10^{-10}$  at the same pressure and temperature in the local thermodynamic equilibrium case). However, above  $10^{-3}$  bar, it is rapidly photo-dissociated into 2S. The outcome is a quick drop-off in its abundance at all temperatures.

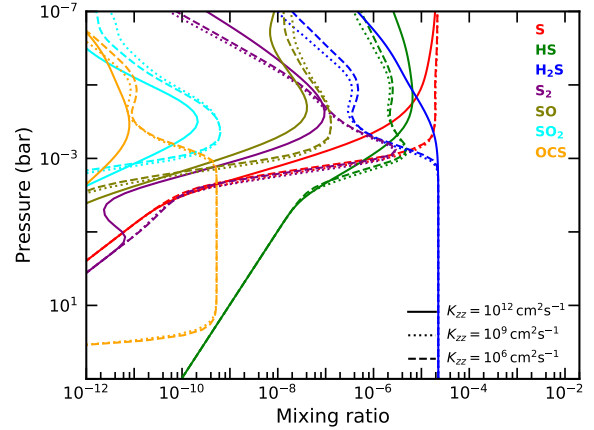


**Figure 6.** Sulfur chemistry in a 1200 K isothermal hot Jupiter atmosphere. This model explores the sensitivity of sulfur chemistry to the strength of the vertical mixing, by comparing models with three different  $K_{zz}$  values. This atmosphere has a solar metallicity, a gravity of  $10 \text{ ms}^{-2}$  and has a UV spectrum  $10\times$  Earth's applied to it.

$\text{OCS}$  is not greatly affected by the introduction of disequilibrium chemistry. Its abundance is still determined by the reaction between HS and CO.

### 4.3 Diffusion Strength

It is important to understand how our choices for the parameters of the disequilibrium chemistry can affect the overall distribution of sulfur chemistry in planetary atmospheres. To that effect, in Figure 6, we compare three atmospheric models of a 1200 K isothermal hot Jupiter with different strengths of eddy-diffusion,  $K_{zz}$ . We do so to test the sensitivity of sulfur chemistry to the strength of the vertical mixing in the atmosphere. We chose to use two extremes of diffusion,  $K_{zz} = 10^6 \text{ cm}^2 \text{ s}^{-1}$  (Dashed) and  $K_{zz} = 10^{12} \text{ cm}^2 \text{ s}^{-1}$  (Solid), to understand the limiting cases for diffusion. We also include the previously used average case of  $K_{zz} = 10^9 \text{ cm}^2 \text{ s}^{-1}$  (Dotted) as a comparison.

Immediately seen is that the weakest mixing,  $K_{zz} = 10^6 \text{ cm}^2 \text{ s}^{-1}$ , does not differ greatly from the intermediate case of  $K_{zz} = 10^9 \text{ cm}^2 \text{ s}^{-1}$ . This suggests that  $K_{zz} = 10^9 \text{ cm}^2 \text{ s}^{-1}$  is already sufficiently low that eddy-diffusion is having little effect upon sulfur chemistry.

For the stronger diffusion,  $K_{zz} = 10^{12} \text{ cm}^2 \text{ s}^{-1}$ , there are several significant differences to the abundance of sulfur molecules. Most of these effects stem from the diffusion quenching the  $\text{H}_2\text{S}$ , such that it stays as the most abundant sulfur molecule up until  $10^{-5}$  bar. This results in a lower atomic S abundance, which has a knock-on effect of also lowering the abundance of both SO and  $\text{SO}_2$ .

The sulfur allotrope  $\text{S}_2$  is also significantly affected by the stronger diffusion. Its abundance between  $10^{-1}$  bar and  $10^{-4}$  bar drops by up to two orders of magnitude compared to the weaker diffusion cases. This is largely caused by the  $\text{S}_2$  diffusing higher into the atmosphere where it can be photo-dissociated, which causes the drop-off in abundance from  $10^{-1}$  bar. Above  $10^{-4}$  bar, the stronger diffusion lifts the abundance of  $\text{S}_2$  faster than it can be dissociated, to mixing ratios slightly above that of the weaker diffusion models.

Overall, the strength of the vertical mixing does not have much

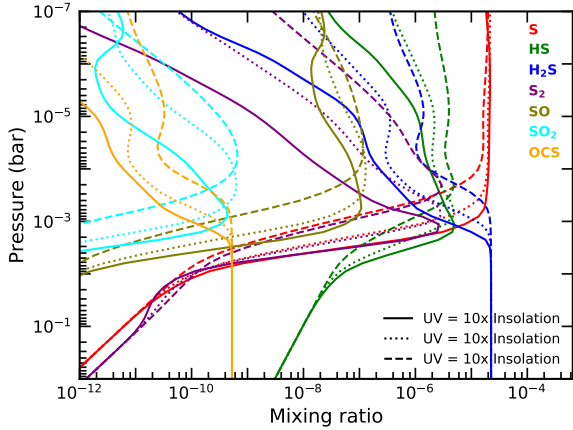


**Figure 7.** Sulfur chemistry in a 1200 K isothermal hot Jupiter atmosphere. This model explores the sensitivity of sulfur chemistry to the strength of the UV flux, by comparing models with three different strength of UV. This atmosphere has a solar metallicity,  $K_{zz} = 10^9 \text{ cm}^2 \text{ s}^{-1}$  and a gravity of  $10 \text{ ms}^{-2}$ .

impact on most sulfur molecules. However, strong mixing may be able to keep  $\text{H}_2\text{S}$  detectable higher in the atmosphere, but strong mixing also significantly suppresses the abundance of  $\text{S}_2$ , preventing its abundance from reaching detectable levels.

#### 4.4 UV Strength

We also examine how altering the strength of the UV flux being applied to the top of the model can alter the sulfur chemistry. While this is not a very realistic change to be made independent of all other parameters, (since the flux strength is most commonly set by the distance of the planet from the star, which would greatly impact the atmosphere’s temperature), it is important to understand our network’s sensitivity to changes in the rate of photochemistry. As such, we present three different models of a hot Jupiter with a 1200 K isothermal atmosphere in Figure 7. Two have extremes of UV irradiation at  $100\times$  Earth’s (Solid) and  $1\times$  Earth’s (Dashed). The other has  $10\times$  Earth’s (Dotted) irradiation, the same as previously used in this section.

Most species show no change deep in the atmosphere, below the  $10^{-2}$  bar level. No species show any difference below  $10^{-1}$  bar. This shows that even for extreme irradiation, the deepest parts of the atmosphere are difficult to move away from thermochemical equilibrium.

The species primarily affected by the change in UV flux is  $\text{H}_2\text{S}$ . Its abundance drops by an order of magnitude at  $10^{-3}$  bar for the highest flux compared to the lowest flux. This also greatly impacts the S at the same pressure. Its abundance is up to five orders of magnitude greater for the greatest flux compared to the smallest. This difference is only seen for a small pressure window however, and the abundance of S is very similar across all three fluxes above  $10^{-4}$  bar.

In this same pressure window, the greater availability of S caused by the stronger flux allows the abundance of both SO and  $\text{SO}_2$  to grow much larger than in the models with weaker fluxes. However, above  $10^{-4}$  bar this is reversed as the available S becomes similar in all three models, resulting in the strongest UV model depleting SO and  $\text{SO}_2$  by about an order of magnitude compared to the weakest UV model.

The comparative abundance of  $\text{S}_2$  goes through several phases. Deep in the atmosphere, around  $10^{-1}$  bar, the stronger UV flux can penetrate deep enough to begin to dissociate it into 2S. However, not far above this, around  $10^{-2}$  bar, the excess S that are produced by  $\text{H}_2\text{S}$  dissociation in the stronger UV cases are sufficient to boost the production of  $\text{S}_2$  above its rate of photo-dissociation. Thus we see more  $\text{S}_2$  in the stronger UV model, up until between  $10^{-3}$  bar and  $10^{-4}$  bar when the availability of atomic S equalises across all three models. Above this, the stronger UV flux once again dominates in dissociating  $\text{S}_2$ , resulting in its abundance being several orders of magnitude lower than in the weak UV model.

Overall, the strength of the UV flux simply shifts the abundance profiles deeper into the atmosphere. This happens because the stronger flux can penetrate deeper, with an increase of two orders of magnitude in UV flux able to push the profiles of sulfur molecules one order of magnitude deeper in pressure into the atmosphere.

## 5 SULFUR’S IMPACT ON ATMOSPHERIC CNO-CHEMISTRY

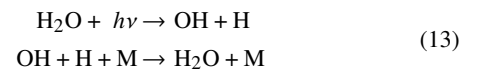
In this section we investigate what effect the sulfur chemistry has upon the composition of both the hot Jupiter HD 209458b and the warm Jupiter 51 Eri b. We compare atmospheric models of these planets with and without sulfur included in our network. In this way we isolate sulfur’s impact, and examine the pathways in our network that lead to these differences occurring.

### 5.1 HD 209458 b

We chose to examine the effects of sulfur chemistry on the atmosphere of the well studied hot Jupiter, HD 209458b. We have previously investigated this planet with LEVI in Hobbs et al. (2019), and we return to it again. We do so now with our updated chemical model to discover how the inclusion of sulfur chemistry affects the predicted abundance profiles of this hot Jupiter’s atmosphere.

As can be seen in Figure 8, we see no difference due to the inclusion of sulfur below 1 bar, in the deep atmosphere of the planet. At this depth, the abundance of the main sulfur species is set by the same reaction path as shown in Reaction 3. These reactions are very rapid and interactions with other species are slow by comparison, preventing sulfur from having any effect on CNO chemistry in the deep atmosphere.

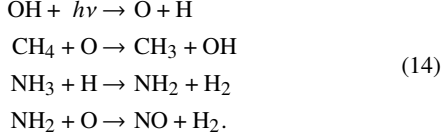
Higher in the atmosphere, around  $10^{-3}$  bar, sulfur has a much more significant effect on the CNO chemistry. In Figure 8, it can be seen that at this pressure the inclusion of sulfur decreases the predicted abundance of  $\text{NH}_3$ ,  $\text{CH}_4$  and HCN by up to two orders of magnitude. In a sulfur free atmosphere, the dominant pathway for  $\text{CH}_4$  and  $\text{NH}_3$  destruction is via the photolysis of water



As shown in Figure 8 large amounts of both the OH and H are produced in an atmosphere with a high UV flux. At this height in the atmosphere, the vast majority of OH and H quickly reform back to  $\text{H}_2\text{O}$  via a three body reaction, preventing any significant

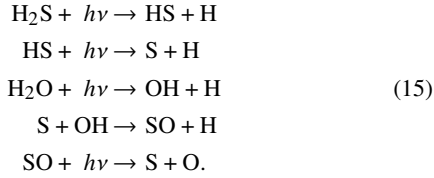


depletion of it. However, some OH can be further photolysed into atomic O and H, that can then react with further molecules,

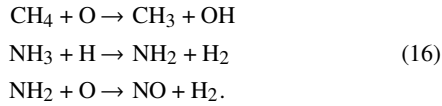


In particular, the liberated O radical can react with CH<sub>4</sub>, and the H radical with NH<sub>3</sub>, followed by the O radical with NH<sub>2</sub>. These are effective pathways to deplete CH<sub>4</sub> and NH<sub>3</sub>, since although the radicals CH<sub>3</sub> and NO can be restored to the initial molecules by the reverse reaction, they most often go on to form other species.

With the inclusion of S in the atmosphere, a new, more efficient route that leads to the destruction of CH<sub>4</sub> and NH<sub>3</sub> appears



Within this new pathway, the complete photolysis of H<sub>2</sub>S produces additional H and a large pool of free S atoms. These S atoms are part of a cycle that reacts with the short lived OH to produce SO, which is then photo-dissociated to S and O. The pathway that subsequently destroys NH<sub>3</sub> and CH<sub>4</sub> is identical to that of a sulfur free atmosphere



However, the important distinction is in the steady state abundance of OH and O: In a sulfur free atmosphere the steady state abundance of OH is up to 30× lower than in an atmosphere with sulfur, since OH can't effectively build up. Without sulfur, OH generally reacts back to H<sub>2</sub>O with some of it being dissociated to start the pathway of NH<sub>3</sub> and CH<sub>4</sub> destruction. However, in an atmosphere containing sulfur, OH reacts with S to create the much more stable species SO, that is susceptible to photo-dissociation. The O production from this dissociation results in a steady state abundance of O that is 30 times larger than in a sulfur free atmosphere. This much larger pool of O can react with CH<sub>4</sub>, NH<sub>2</sub> and other H bearing species. This significantly reduces the abundance of CH<sub>4</sub> and NH<sub>3</sub> compared to a sulfur free atmosphere, and enhances the OH steady state abundance by 5-10x.

Figure 8 shows that, at pressures lower than 10<sup>-5</sup> bar, the effects of sulfur once again become insignificant. The reaction H + OH → H<sub>2</sub> + O produces atomic O at a rate several orders of magnitude faster than the production and subsequent photo-dissociation of SO. As a result, the pathways that lead to the destruction of CH<sub>4</sub> and NH<sub>3</sub> at this height are no longer dependant on sulfurs presence. As such, the very upper atmospheres of hot Jupiters that contain sulfur looking nearly indistinguishable from those without sulfur.

There is potential for detecting the differences caused by the inclusion of sulfur in hot Jupiters' atmospheres. There has already been evidence for CH<sub>4</sub> (Guilluy et al. 2019) and HCN (Hawker et al. 2018; Cabot et al. 2019) detections in the atmosphere's of hot Jupiters. Most retrievals identify species, and their abundances,

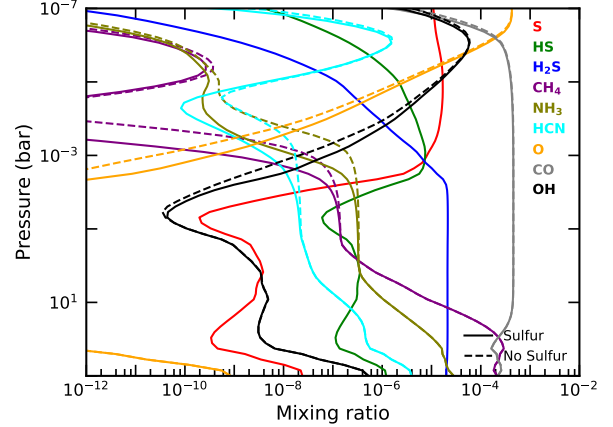


**Figure 8.** A comparison of the abundance profiles for the hot Jupiter HD 209458b both with (solid lines) and without (dashed lines) our new sulfur network being included. This model uses the pressure - temperature profile and  $K_{zz}$  profile from Hobbs et al. (2019). It has solar metallicity, a gravity of 9.36 ms<sup>-2</sup> and has a UV spectrum 800× Earth's applied to it.

around the pressure of 10<sup>-3</sup> bar. Thus, it should be possible to detect the drop in abundance of these molecules due to sulfur. However, the pressure range over which there is an identifiable difference due to sulfur is rather limited. Any investigated spectra of this planet would need to be very precise, more so than any currently obtainable.

## 5.2 Warm Jupiters

Previously, there has been discussion in the literature about how sulfur on warm Jupiters may affect the abundance of species in the atmosphere of these planets. Of particular note is the warm Jupiter 51 Eri b, which both Moses et al. (2016) and Zahnle et al. (2016) have modelled in the past. Moses et al. (2016) ran models without any sulfur in the atmosphere, while Zahnle et al. (2016) ran models with sulfur. When comparing between the two models, Zahnle et al. (2016) found up to two orders of magnitude less CO<sub>2</sub> than the model of Moses et al. (2016). In this section, we run our model for the atmosphere of 51 Eri b using the pressure temperature profile and stellar UV flux of Moses et al. (2016). However, unlike in Moses et al. (2016), we use a constant  $K_{zz} = 10^7$  cm<sup>2</sup>s<sup>-1</sup>. The atmosphere of 51 Eri b is modelled as having solar metallicity and has a constant gravity of 32 ms<sup>-2</sup>. In Figure 9 we compare two models, with and without sulfur. Because the temperature of 51 Eri b falls below 500 K, the lower limit for convergence of our model, LEVI, we solve for this atmosphere using ARGO (Rimmer & Helling 2016).

Our results clearly show that the CO<sub>2</sub> abundance in a sulfurous atmosphere is significantly depleted, with peak CO<sub>2</sub> abundance five times less than in a non-sulfurous atmosphere. This is less than the difference seen between Zahnle et al. (2016) and Moses et al. (2016). Our results for CO<sub>2</sub> overall agree better with Moses et al. (2016), both with and without sulfur. However, the reason for the decrease in CO<sub>2</sub> abundance with the inclusion of sulfur is the effect of the

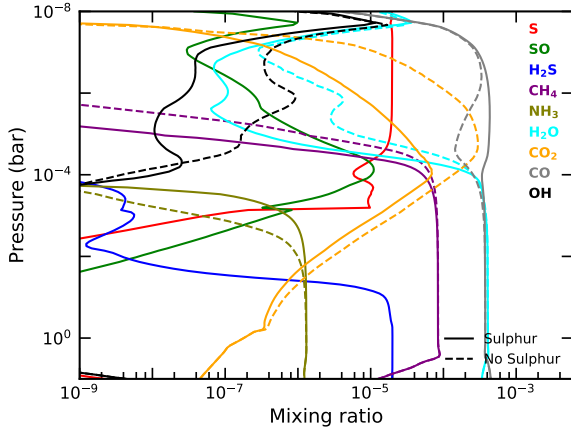
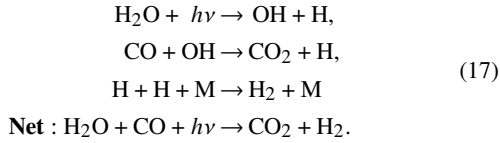
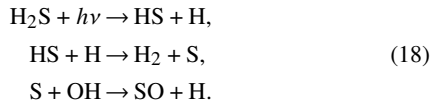


**Figure 9.** A comparison of the abundance profiles for a warm Jupiter model both with (solid lines) and without (dashed lines) our new sulfur network being included. This warm Jupiter uses the P-T profile and UV spectrum from [Moses et al. \(2016\)](#). It has a gravity of  $32 \text{ ms}^{-2}$ , a solar metallicity and a constant  $K_{zz} = 10^7 \text{ cm}^2 \text{ s}^{-1}$ .

products of  $\text{H}_2\text{S}$  photo-dissociation on the abundance of OH. Both with and without sulfur,  $\text{CO}_2$  is produced by the following reactions

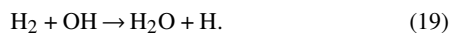


The destruction is also the same regardless of the presence of sulfur, through the photo-dissociation of  $\text{CO}_2$ . What does change is the abundance of OH, which is consumed by reacting with S via



The SO will diffuse upward, where it will photo-dissociate, releasing more atomic sulfur which will consume more hydroxyl radicals. It is this effect of the sulfur chemistry on the hydroxyl radicals that causes the lower abundance of  $\text{CO}_2$  when sulfur is included. The destruction of OH via the photochemical properties of  $\text{H}_2\text{S}$  explains the shift of the peak of  $\text{CO}_2$  to higher pressures when sulfur is present.

There is one other feature of note, the  $\text{H}_2\text{O}$  spike near  $10^{-8}$  bar. This occurs because our constant  $K_{zz}$  places the CO homopause at  $\sim 10^{-7}$  bar. As the CO drops off, it stops effectively self-shielding, and so CO is easily dissociated into  $\text{C}(^1\text{D})$  and  $\text{O}(^1\text{D})$ . The  $\text{O}(^1\text{D})$  reacts with  $\text{H}_2$  to form  $\text{H}_2\text{O}$ .  $\text{H}_2\text{O}$  is preserved at this height, because its destruction forms OH which quickly reacts with  $\text{H}_2$  to reform  $\text{H}_2\text{O}$



This reaction dominates instead of the reaction  $\text{CO} + \text{OH} \rightarrow \text{CO}_2 + \text{H}$  (See Reaction 17) since the depletion of CO due to molecular diffusion means that it is no longer as efficient. This leads to  $\text{H}_2\text{O}$  peaking at  $\sim 10^{-8}$  bar. It drops off above this height because

of a combination of molecular diffusion of  $\text{H}_2\text{O}$  and photochemical destruction of OH.

## 6 SUMMARY AND DISCUSSION

Our goal in this work was to construct a complete sulfur chemical network that would primarily function for the high temperatures of hot Jupiters, but that should be applicable over a large range of temperatures. By combining this network with our chemical kinetics code, LEVI, described in [Hobbs et al. \(2019\)](#) and the H/C/O/N network STAND2019 from [Rimmer & Helling \(2016\)](#) and [Rimmer & Rugheimer \(2019\)](#) we gained the ability to find the steady-state solutions for chemical abundance in the atmospheres of a variety of hot Jupiters. We validated our new network against other previously produced similar models to compare and contrast the similarities and differences. We investigated the primary pathways of sulfur chemistry over a range of hot Jupiter models, and examined how the abundance of sulfur species changed with variations to the model. We also compared how the inclusion of sulfur into a hot Jupiter's atmosphere can affect the abundance of other, non-sulfur species, potentially altering these species detectability.

We validated our network against the network first shown in [Zahnle et al. \(2009\)](#) (Figure 2). We found that although variations existed between the atmospheric abundance profiles, there were good explanations for them. In the deep atmosphere, the divergences are due to different thermochemical constants between the two models. Later publications from the same group ([Evans et al. 2018](#)) have converged to have similar results to our network in this portion of the atmosphere (Figure 3). In the upper atmosphere, the species' abundances follow the same general trends, though they do not match exactly. This is inferred to be due to different choices in the rate constants for the reactions in the network. This result emphasises the need for new measurements of these rates, without which it will not be possible to know the correct reactions, and rate constants, to use to create an accurate network.

Across a range of isothermal hot Jupiter atmospheres, we investigated the most abundant sulfur species and how this varies with the model's parameters. In our disequilibrium atmosphere model (Figure 5) we found that from the bottom of the atmosphere until between  $10^{-2}$  and  $10^{-3}$  bar,  $\text{H}_2\text{S}$  contains nearly all of the atmosphere's sulfur. Above this,  $\text{H}_2\text{S}$  is destroyed by photochemically produced H radicals that cause atomic S to become the primary sulfur carrier for the rest of the atmosphere. Other sulfur molecules of note are  $\text{S}_2$  and HS.  $\text{S}_2$  builds up significantly around  $10^{-3}$  bar, particularly on slightly cooler hot Jupiters, where for a brief pressure window it is the most abundant sulfur species. The mercapto radical, HS, is one of the few sulfur molecules whose presence may have already been detected on an exoplanet ([Evans et al. 2018](#)). We find that it builds up strongly around  $10^{-3}$  bar, especially along isotherms  $> 1200 \text{ K}$ , with a maximum abundance of  $4 \times 10^{-3}$  seen in our model in Figure 5.

We also examined the sensitivity of sulfur chemistry to variations in both the strength of the vertical mixing (Figure 6) and the strength of the UV flux (Figure 7) applied to the atmosphere. We found that weakening the diffusion had little effect on the sulfur species. Stronger mixing increased the abundance of  $\text{H}_2\text{S}$  above  $10^{-3}$  bar, while decreasing the abundance of S and  $\text{S}_2$ . The effect of stronger UV irradiation is primarily to dissociate photosensitive molecules deeper into the atmosphere. Species such as  $\text{H}_2\text{S}$  were up to two orders of magnitude less abundant at  $10^{-3}$  bar in more highly irradiated models.

Most sulfur species are not easily detected in exoplanet atmospheres, but that does not mean that sulfur chemistry does not matter for atmospheric retrievals. Our models have shown that the presence of sulfur in both hot and warm Jupiter atmospheres can significantly change the abundance of other, more easily detected, molecules. Of particular note are the differences we have found to the abundances of CH<sub>4</sub>, HCN and NH<sub>3</sub> in hot Jupiters by including S in the network, as well as CO<sub>2</sub> in warm Jupiters. We found that around a pressure of 10<sup>-3</sup> bar in a atmospheric model of HD 209458b (Figure 8), the abundances of NH<sub>3</sub>, CH<sub>4</sub> and HCN in a sulfurous atmosphere dropped by several orders of magnitude when compared to their abundances in a non-sulfurous atmosphere. This is a very large change, but it occurs over a very narrow pressure window. If this intersects with the detectable range made by observations, it would be a significant and noticeable effect. But, if the detection occurred at location higher or lower in the atmosphere, no change would be noticed compared to a sulfur free case. It is also very likely that the location at which sulfur chemistry impacts these molecules is dependant upon many of the planet's parameters: The planet's temperature and metallicity, as well as the diffusion strength or the incoming UV flux. More testing and modelling is required to discover exactly how these parameters will alter sulfur's effect upon these molecules. The effect of sulfur upon CO<sub>2</sub> in warm Jupiters is also important, first noticed when comparing the sulfurous (Zahnle et al. 2016) and non-sulfurous (Moses et al. 2016) models of 51 Eri b. We find our network predicts up to five times less CO<sub>2</sub>, due to sulfur, above 10<sup>-4</sup> bar. Below this pressure, the loss is present, but less significant. In this section of the upper atmosphere, we predict approximately half an order of magnitude more CO<sub>2</sub> compared to the model in Zahnle et al. (2016). This is again down to uncertainties in the rate constants used for our sulfur reactions.

Current observations may struggle to distinguish the effects of sulfur we predict in both hot and warm Jupiters. It is important that observations from the next generation of telescopes take these effects into account, since they can significantly alter the composition of the atmosphere.

However, firm conclusions of the precise effects of sulfur can be difficult to make, due to how many uncertainties there are in the reaction rates within the network. As we have shown, these rates can greatly affect not just other sulfur species, but other detectable species within the atmosphere. New measurements of the rates of these sulfur reactions need to take place to truly be able to constrain the exact effect that sulfur can have. Some of the most important reactions discussed within this work still have large divergences between their different measurements. Because of this, we focus next on where some of these reactions' rates come from.

### Photochemistry of H<sub>2</sub>S

The photo-dissociation of H<sub>2</sub>S is one of two photochemical sulfur reactions that form the explanation for sulfur's significant impact on other species in warm and hot Jupiters. There are a large number of works that have measured its UV cross-section, though not all of them agree what that cross-section should be. The work of Lee et al. (1987) provides an effective "backbone" to the wavelength-dependent absorption cross-sections for H<sub>2</sub>S, and provides the lowest measured estimates for H<sub>2</sub>S absorption of all observations, diverging from other measurements at  $\lambda < 172$  nm. Both Watanabe & Jursa (1964) and Wu & Chen (1998) find cross-sections below 172 nm that are a factor of 2-3 greater. Thompson et al. (1966) measures the absorption cross-section between 180 nm and 214 nm, in good agreement with other measurements at these wavelengths, though with a slight divergence between 210–214 nm. Wu & Chen (1998) generally agrees with most other measurements wherever

one of the measurements diverges, and matches a measurement at a single (250 nm) wavelength very well (Wight & Leone 1983). The measurements of Wu & Chen (1998) are clean and the results suggest few systematics and a very deep noise floor. For this reason the JPL database recommends using their H<sub>2</sub>S cross-sections. More recently, Grosch et al. (2015) has made measurements at a higher resolution. These measurements diverge from Wu & Chen (1998) by a factor of 5 between 250 and 260 nm, suggesting the higher resolution has come at the cost of a higher noise floor.

### Photo-chemistry of SO

The photo-dissociation of SO is the second of the important photochemical sulfur reactions. The most accurate cross-sections for SO were compiled by the Leiden database (Heays et al. 2017), based on Phillips (1981); Nee & Lee (1986); Norwood & Ng (1989). The cross-sections all agree with each other reasonably well.

### H + SH -> H<sub>2</sub> + S vs H<sub>2</sub> + S -> H + SH

We found that the reaction H + SH  $\longrightarrow$  H<sub>2</sub> + S was significant in the pathway that lead to CO<sub>2</sub> destruction in 51 Eri b's atmosphere. However, in our network we choose to use this reaction's reverse, H<sub>2</sub> + S  $\longrightarrow$  H + SH, even though it has an activation barrier. Our justification for this is that for H + SH  $\longrightarrow$  H<sub>2</sub> + S all the results are at room temperature, and all of them were measured in the 1970's and 1980's.

Cupitt & Glass (1970) performed a flow discharge with H<sub>2</sub>S and O<sub>2</sub>, and estimated the rate to be  $k = 1.3 \times 10^{-10} \text{ cm}^3 \text{ s}^{-1}$ . The experiment was subsequently revisited, and the rate constant corrected to  $k = 2.51 \times 10^{-11} \text{ cm}^3 \text{ s}^{-1}$  in (Cupitt & Glass 1975).

Bradley et al. (1973) also performed a flow discharge with H<sub>2</sub>S, controlling the overall reaction with NO, attempting to isolate the individual reactions, and constrained the HS hydrogen abstraction reaction to  $k = 4.15 \times 10^{-11} \text{ cm}^3 \text{ s}^{-1}$ . Their results do not indicate any kinetic barrier or polynomial temperature dependence.

Tiee et al. (1981) used a 193 nm UV laser to dissociate H<sub>2</sub>S, forming HS, and then subsequently measured the decay of HS. They found a maximum rate of  $k < 1.69 \times 10^{-11} \text{ cm}^3 \text{ s}^{-1}$ .

Nicholas et al. (1979) used radio-frequency pulse discharge and found the measurement of HS decay to be  $k = 2.16 \times 10^{-11} \text{ cm}^3 \text{ s}^{-1}$ .

Langford & Oldershaw (1972) used flash photolysis and made the measurement of the HS decay to be  $k = 1.1 \times 10^{-11} \text{ cm}^3 \text{ s}^{-1}$ .

These rates are very variable and none of them consider the temperature dependence of the reaction. In contrast, the reverse reaction, H<sub>2</sub> + S  $\longrightarrow$  H + SH, was constrained much better by two experiments in the late 1990's. They were performed over a much larger temperature range, one more applicable to hot Jupiters.

Woiki & Roth (1995) used OCS/H<sub>2</sub> pyrolysis and CS<sub>2</sub>/H<sub>2</sub> photolysis to generate S atoms that could then react with H<sub>2</sub>. They found the reaction rate to be  $k = 9.96 \times 10^{-10} \exp(-12070\text{K}/T) \text{ cm}^3 \text{ s}^{-1}$  for a temperature range of 1257 K to 3137 K.

Shiina et al. (1996) studied the thermal decomposition of H<sub>2</sub>S and its subsequent reactions, and found the reaction between H<sub>2</sub> and S to be  $k = 2.62 \times 10^{-10} \exp(-9920\text{K}/T) \text{ cm}^3 \text{ s}^{-1}$  over a temperature range of 1050 K to 1660 K.

As a result we decided that using the reaction H<sub>2</sub> + S  $\longrightarrow$  H + SH in our network was the choice offering the greatest accuracy in modelling hot Jupiters.

### OH + S -> H + SO

This reaction is the last reaction important to explaining the impact of sulfur in hot and warm Jupiters. It has been mentioned in several reviews, all based on a single experimental measurement by Jourdain et al. (1979). They used a flow discharge with SO<sub>2</sub> and H<sub>2</sub>O, and found  $k = 6.95 \times 10^{-11} \text{ cm}^3 \text{ s}^{-1}$ . Without a second measurement, it is difficult to determine this reaction's uncertainties,

and without uncertainties, there is no way to perform a sensitivity analysis accurately.

Finally, it is important to consider that while it is difficult to identify the bulk sulfur abundance without the detection of sulfur species, the effect of sulfur upon other species can be used as a method to constrain the sulfur abundance. There of course would be a large degree of degeneracy in this parameter, but it could work as a first step to limiting the sulfur abundance of exo-planets to realistic values.

## ACKNOWLEDGEMENTS

R.H. and O.S. acknowledge support from the UK Science and Technology Facilities Council (STFC). P.B.R. thanks the Simons Foundation for funding (SCOL awards 599634)

## DATA AVAILABILITY

The data underlying this article is available in the article.

## REFERENCES

- Agúndez M., Parmentier V., Venot O., Hersant F., Selsis F., 2014, *A&A*, **564**, A73
- Amano A., Yamada M., Hashimoto K., Sugiura K., 1983, *NIPPON KAGAKU KAISHI*, 1983, 385
- Asplund M., Grevesse N., Sauval A. J., Scott P., 2009, *ARA&A*, **47**, 481
- Atkinson R., Baulch D. L., Cox R. A., Hampson R. F., Kerr J. A., Troe J., 1992, *Journal of Physical and Chemical Reference Data*, **21**, 1125
- Atkinson R., et al., 2004, *Atmospheric Chemistry and Physics*, **4**, 1461
- Bauer S., Jeffers P., Lifshitz A., Yadava B., 1971, *Symposium (International) on Combustion*, **13**, 417
- Black G., Jusinski L., Slanger T., 1983, *Chemical Physics Letters*, **102**, 64
- Blitz M. A., Hughes K. J., Pilling M. J., Robertson S. H., 2006, *The Journal of Physical Chemistry A*, **110**, 2996
- Bradley J. N., Trueman S. P., Whytock D. A., Zaleski T. A., 1973, *Journal of the Chemical Society, Faraday Transactions 1: Physical Chemistry in Condensed Phases*, **69**, 416
- Bulatov V., Vereshchuk S., Dzegilenko F., Sarkisov O., Khabarov V., 1990, *KHIMICHESKAYA FIZIKA*, **9**, 1214
- Cabot S. H. C., Madhusudhan N., Hawker G. A., Gandhi S., 2019, *MNRAS*, **482**, 4422
- Chase M., 1998, NIST-JANAF Thermochemical Table. American Institute of Physics
- Chung K., Calvert J. G., Bottenheim J. W., 1975, *International Journal of Chemical Kinetics*, **7**, 161
- Cooper W. F., Hershberger J. F., 1992, *The Journal of Physical Chemistry*, **96**, 5405
- Craven W., Murrell J. N., 1987, *J. Chem. Soc., Faraday Trans. 2*, **83**, 1733
- Cupitt L., Glass G., 1970, *Transactions of the Faraday Society*, **66**, 3007
- Cupitt L., Glass G., 1975, *Int. J. Chem. Kinet.:(United States)*, **7**
- Demore W., et al., 1997, JPL Publication, 90
- Dorthe G., Caubet P., Vias T., Barrere B., Marchais J., 1991, *The Journal of Physical Chemistry*, **95**, 5109
- Drummond B., Mayne N. J., Manners J., Baraffe I., Goyal J., Tremblin P., Sing D. K., Kohary K., 2018, *ApJ*, **869**, 28
- Du S., Francisco J. S., Shepler B. C., Peterson K. A., 2008, *The Journal of chemical physics*, **128**, 204306
- Evans T. M., et al., 2018, *AJ*, **156**, 283
- Gao P., Marley M. S., Zahnle K., Robinson T. D., Lewis N. K., 2017, *AJ*, **153**, 139
- Garland N. L., 1998, *Chemical Physics Letters*, **290**, 385
- Goumri A., Rocha J.-D. R., Marshall P., 1995, *The Journal of Physical Chemistry*, **99**, 10834
- Goumri A., Rocha J.-D. R., Laakso D., Smith C. E., Marshall P., 1999, *The Journal of Physical Chemistry A*, **103**, 11328
- Grosch H., Fateev A., Clausen S., 2015, *J. Quant. Spectrosc. Radiative Transfer*, **154**, 28
- Guilluy G., Sozzetti A., Brogi M., Bonomo A. S., Giacobbe P., Claudi R., Benatti S., 2019, *A&A*, **625**, A107
- Hawker G. A., Madhusudhan N., Cabot S. H. C., Gandhi S., 2018, *ApJ*, **863**, L11
- He C., et al., 2020, in AAS/Division for Planetary Sciences Meeting Abstracts. p. 403.04
- Heays A. N., Bosman A. D., van Dishoeck E. F., 2017, *A&A*, **602**, A105
- Herndon S. C., Froyd K. D., Lovejoy E. R., Ravishankara A. R., 1999, *The Journal of Physical Chemistry A*, **103**, 6778
- Hindiyarti L., Glarborg P., Marshall P., 2007, *The Journal of Physical Chemistry A*, **111**, 3984
- Hobbs R., Shorttle O., Madhusudhan N., Rimmer P., 2019, *MNRAS*, **487**, 2242
- Hodgskiss M. S. W., Crockford P. W., Peng Y., Wing B. A., Horner T. J., 2019, *Proceedings of the National Academy of Science*, **116**, 17207
- Hu R., Seager S., Bains W., 2012, *ApJ*, **761**, 166
- Hu R., Seager S., Bains W., 2013, *ApJ*, **769**, 6
- Hwang S. M., Cooke J. A., De Witt K. J., Rabinowitz M. J., 2010, *International Journal of Chemical Kinetics*, **42**, 168
- Irwin P. G. J., 1999, *Surveys in Geophysics*, **20**, 505
- Isshiki N., Murakami Y., Tsuchiya K., Tezaki A., Matsui H., 2003, *The Journal of Physical Chemistry A*, **107**, 2464
- Jourdain J., Bras G. L., Combourieu J., 1979, *International Journal of Chemical Kinetics*, **11**, 569
- Krasnopolsky V. A., 2007, *Icarus*, **191**, 25
- Krasnopolsky V. A., 1994, *Icarus*
- Kurbanov M., Mamedov K., 1995, *Kinetics and Catalysis - KINET CATAL-ENGL TR*, **36**, 455
- Kurten T., Lane J. R., Jorgensen S., Kjaergaard H. G., 2010, *Phys. Chem. Chem. Phys.*, **12**, 12833
- Langford R., Oldershaw G., 1972, *Journal of the Chemical Society, Faraday Transactions 1: Physical Chemistry in Condensed Phases*, **68**, 1550
- Lee L. C., Wang X., Suto M., 1987, *J. Chem. Phys.*, **86**, 4353
- Liang M.-C., Parkinson C. D., Lee A. Y. T., Yung Y. L., Seager S., 2003, *ApJ*, **596**, L247
- Lilenfeld H. V., Richardson R. J., 1977, *The Journal of Chemical Physics*, **67**, 3991
- Lodders K., Fegley B., 2002, *Icarus*, **155**, 393
- Lu C.-W., Wu Y.-J., Lee Y.-P., 2003, *Journal of Physical Chemistry A - J PHYS CHEM A*, **107**
- Lu C.-W., Wu Y.-J., Lee Y.-P., Zhu R. S., Lin M. C., 2006, *The Journal of Chemical Physics*, **125**, 164329
- Macdonald F. A., Wordsworth R., 2017, *Geophys. Res. Lett.*, **44**, 1938
- Malin G., 1997, *Nature*, **387**, 857
- Mills F., 1998, I. Observations and Photochemical Modeling of the Venus Middle Atmosphere. II. Thermal Infrared Spectroscopy of Europa and Callisto
- Miyoshi A., Shiina H., Tsuchiya K., Matsui H., 1996, *Symposium (International) on Combustion*, **26**, 535
- Montoya A., Sendt K., Haynes B. S., 2005, *The Journal of Physical Chemistry A*, **109**, 1057
- Moses J. I., Allen M., Gladstone G. R., 1995, *Geophys. Res. Lett.*, **22**, 1597
- Moses J. I., Zolotov M. Y., Fegley B., 2002, *Icarus*, **156**, 76
- Moses J. I., et al., 2011, *ApJ*, **737**, 15
- Moses J. I., et al., 2016, *ApJ*, **829**, 66
- Mousavipour S. H., Namdar-Ghanbari M. A., Sadeghian L., 2003, *The Journal of Physical Chemistry A*, **107**, 3752
- Nee J. B., Lee L. C., 1986, *J. Chem. Phys.*, **84**, 5303
- Nicholas J. E., Amodio C. A., Baker M. J., 1979, *Journal of the Chemical Society, Faraday Transactions 1: Physical Chemistry in Condensed Phases*, **75**, 1868
- Norwood K., Ng C. Y., 1989, *Chemical Physics Letters*, **156**, 145

Penzhorn R.-D., Canosa C., 1983.  
 Phillips L. F., 1981, *Journal of Physical Chemistry*, **85**, 3994  
 Richardson R., 1975, *The Journal of Physical Chemistry*, **79**, 1153  
 Rimmer P. B., Helling C., 2016, *ApJS*, **224**, 9  
 Rimmer P. B., Rugheimer S., 2019, *Icarus*, **329**, 124  
 Rimmer P. B., Jordan S., Constantinou T., Woitke P., Shorttle O., Hobbs R., Paschodimas A., 2021, *The Planetary Science Journal*, p. submitted  
 Sander S., et al., 2006, Chemical kinetics and photochemical data for use in atmospheric studies evaluation number 15  
 Schofield K., 1973, *Journal of Physical and Chemical Reference Data*, **2**, 25  
 Sendt K., Haynes B. S., 2005, *The Journal of Physical Chemistry A*, **109**, 8180  
 Shiina H., Oya M., Yamashita K., Miyoshi A., Matsui H., 1996, *The Journal of Physical Chemistry*, **100**, 2136  
 Shum L. G. S., Benson S. W., 1985, *International Journal of Chemical Kinetics*, **17**, 749  
 Singleton D. L., Cvetanovic R. J., 1988, *Journal of Physical and Chemical Reference Data*, **17**, 1377  
 Stock J. W., Kitzmann D., Patzer A. B. C., Sedlmayr E., 2018, *MNRAS*, **479**, 865  
 Thompson S. D., Carroll D. G., Watson F., O'Donnell M., McGlynn S. P., 1966, *J. Chem. Phys.*, **45**, 1367  
 Tiee J. J., Wampler F. B., Oldenborg R. C., Rice W. W., 1981, *Chemical Physics Letters*, **82**, 80  
 Titov D. V., Ignatiev N. I., McGouldrick K., Wilquet V., Wilson C. F., 2018, *Space Sci. Rev.*, **214**, 126  
 Tsai S.-M., Lyons J. R., Grosheintz L., Rimmer P. B., Kitzmann D., Heng K., 2017, *ApJS*, **228**, 20  
 Tsuchiya K., Yokoyama K., Matsui H., Oya M., Dupre G., 1994, *The Journal of Physical Chemistry*, **98**, 8419  
 Tsuchiya K., Yamashita K., Miyoshi A., Matsui H., 1996, *The Journal of Physical Chemistry*, **100**, 17202  
 Tsuchiya K., Kamiya K., Matsui H., 1997, *International Journal of Chemical Kinetics*, **29**, 57  
 Vandeputte A. G., Reyniers M.-F., Marin G. B., 2010, *The Journal of Physical Chemistry A*, **114**, 10531  
 Venot O., Hébrard E., Agúndez M., Dobrijevic M., Selsis F., Hersant F., Iro N., Bounaceur R., 2012, *A&A*, **546**, A43  
 Visscher C., Lodders K., Fegley Bruce J., 2006, *ApJ*, **648**, 1181  
 Wakelam V., et al., 2012, *ApJS*, **199**, 21  
 Wakelam V., et al., 2015, *The Astrophysical Journal Supplement Series*, **217**, 20  
 Wang B., Hou H., 2005, *Chemical Physics Letters*, **410**, 235  
 Wang N.-S., Howard C., 1990, *Journal of Physical Chemistry*, **94**, 8787  
 Watanabe K., Jursa A. S., 1964, *J. Chem. Phys.*, **41**, 1650  
 Wei C.-N., Timmons R. B., 1975, *The Journal of Chemical Physics*, **62**, 3240  
 Wight C. A., Leone S. R., 1983, *J. Chem. Phys.*, **79**, 4823  
 Woiki D., Roth P., 1995, *International Journal of Chemical Kinetics*, **27**, 547  
 Wu C. Y. R., Chen F. Z., 1998, *J. Quant. Spectrosc. Radiative Transfer*, **60**, 17  
 Yoshimura M., Koshi M., Matsui H., Kamiya K., Umeyama H., 1992, *Chemical Physics Letters*, **189**, 199  
 Zahnle K., Haberle R. M., Catling D. C., Kasting J. F., 2008, *Journal of Geophysical Research (Planets)*, **113**, E11004  
 Zahnle K., Marley M. S., Freedman R. S., Lodders K., Fortney J. J., 2009, *ApJ*, **701**, L20  
 Zahnle K., Marley M. S., Morley C. V., Moses J. I., 2016, *ApJ*, **824**, 137  
 Zhang X., Liang M. C., Mills F. P., Belyaev D. A., Yung Y. L., 2012, *Icarus*, **217**, 714

**Table A1.** The photo-chemical reactions of the sulphur network used in this work.

No.	Reaction				
1	S <sub>3</sub>	→	S <sub>2</sub>	+	S
2	S <sub>4</sub>	→	S <sub>2</sub>	+	S <sub>2</sub>
3	SO <sub>3</sub>	→	SO <sub>2</sub>	+	O
4	OCS	→	S	+	CO
5	OCS	→	S	+	CO
6	OCS	→	S	+	CO
7	OCS	→	CS	+	O
8	OCS	→	CS	+	O( <sup>1</sup> D)
9	S <sub>2</sub>	→	S	+	S
10	S <sub>2</sub> O	→	SO	+	S
11	S <sub>2</sub> O	→	S <sub>2</sub>	+	O
12	SO	→	S	+	O
13	CS <sub>2</sub>	→	CS	+	S
14	SO <sub>2</sub>	→	SO	+	O
15	SO <sub>2</sub>	→	S	+	O <sub>2</sub>
16	H <sub>2</sub> S	→	HS	+	H
17	CH <sub>3</sub> SH	→	CH <sub>3</sub>	+	HS

## APPENDIX A: THE SULFUR NETWORK

This paper has been typeset from a  $\text{\TeX}/\text{\LaTeX}$  file prepared by the author.

**Table A2.** The 3-body reactions of the sulphur network used in this work.  $\alpha$ ,  $\beta$  and  $\gamma$  (K) refer to the three constants used in the arrhenius equation, such that the rate of reaction is  $k = \alpha(T/300\text{ K})^\beta \exp(-\gamma/T) \text{ m}^3\text{ s}^{-1}$ .

No.	Reaction				$\alpha$	$\beta$	$\gamma$ (K)	Reference
1	S	+	S	$\rightarrow$	S <sub>2</sub>	$3.95 \times 10^{-45}$		Du et al. (2008)
	S	+	S	$\rightarrow$	S <sub>2</sub>	$9.09 \times 10^{-20}$		Du et al. (2008)
2	S	+	S <sub>2</sub>	$\rightarrow$	S <sub>3</sub>	$1.11 \times 10^{-42}$	-2.00	Moses et al. (2002)
	S	+	S <sub>2</sub>	$\rightarrow$	S <sub>3</sub>	$3 \times 10^{-17}$		Moses et al. (2002)
3	S	+	S <sub>3</sub>	$\rightarrow$	S <sub>4</sub>	$1.11 \times 10^{-42}$	-2.00	Moses et al. (2002)
	S	+	S <sub>3</sub>	$\rightarrow$	S <sub>4</sub>	$3 \times 10^{-17}$		Moses et al. (2002)
4	S	+	S <sub>4</sub>	$\rightarrow$	S <sub>5</sub>	$1.11 \times 10^{-42}$	-2.00	Moses et al. (2002)
	S	+	S <sub>4</sub>	$\rightarrow$	S <sub>5</sub>	$3 \times 10^{-17}$		Moses et al. (2002)
5	S	+	S <sub>5</sub>	$\rightarrow$	S <sub>6</sub>	$1.11 \times 10^{-42}$	-2.00	Moses et al. (2002)
	S	+	S <sub>5</sub>	$\rightarrow$	S <sub>6</sub>	$3 \times 10^{-17}$		Moses et al. (2002)
6	S	+	S <sub>6</sub>	$\rightarrow$	S <sub>7</sub>	$1.11 \times 10^{-42}$	-2.00	Moses et al. (2002)
	S	+	S <sub>6</sub>	$\rightarrow$	S <sub>7</sub>	$3 \times 10^{-17}$		Moses et al. (2002)
7	S	+	S <sub>7</sub>	$\rightarrow$	S <sub>8</sub>	$1.11 \times 10^{-42}$	-2.00	Moses et al. (2002)
	S	+	S <sub>7</sub>	$\rightarrow$	S <sub>8</sub>	$3 \times 10^{-17}$		Moses et al. (2002)
8	S <sub>2</sub>	+	S <sub>2</sub>	$\rightarrow$	S <sub>4</sub>	$2.2 \times 10^{-41}$		Nicholas et al. (1979)
	S <sub>2</sub>	+	S <sub>2</sub>	$\rightarrow$	S <sub>4</sub>	$1 \times 10^{-16}$		Nicholas et al. (1979)
9	S <sub>2</sub>	+	S <sub>3</sub>	$\rightarrow$	S <sub>5</sub>	$1.11 \times 10^{-42}$	-2.00	Moses et al. (2002)
	S <sub>2</sub>	+	S <sub>3</sub>	$\rightarrow$	S <sub>5</sub>	$3 \times 10^{-17}$		Moses et al. (2002)
10	S <sub>2</sub>	+	S <sub>4</sub>	$\rightarrow$	S <sub>6</sub>	$1.11 \times 10^{-42}$	-2.00	Moses et al. (2002)
	S <sub>2</sub>	+	S <sub>4</sub>	$\rightarrow$	S <sub>6</sub>	$3 \times 10^{-17}$		Moses et al. (2002)
11	S <sub>2</sub>	+	S <sub>5</sub>	$\rightarrow$	S <sub>7</sub>	$1.11 \times 10^{-42}$	-2.00	Moses et al. (2002)
	S <sub>2</sub>	+	S <sub>5</sub>	$\rightarrow$	S <sub>7</sub>	$3 \times 10^{-17}$		Moses et al. (2002)
12	S <sub>2</sub>	+	S <sub>6</sub>	$\rightarrow$	S <sub>8</sub>	$1.11 \times 10^{-42}$	-2.00	Moses et al. (2002)
	S <sub>2</sub>	+	S <sub>6</sub>	$\rightarrow$	S <sub>8</sub>	$3 \times 10^{-17}$		Moses et al. (2002)
13	S <sub>3</sub>	+	S <sub>3</sub>	$\rightarrow$	S <sub>6</sub>	$1 \times 10^{-42}$		Mills (1998)
	S <sub>3</sub>	+	S <sub>3</sub>	$\rightarrow$	S <sub>6</sub>	$3 \times 10^{-17}$		Mills (1998)
14	S <sub>3</sub>	+	S <sub>4</sub>	$\rightarrow$	S <sub>7</sub>	$1.11 \times 10^{-42}$	-2.00	Moses et al. (2002)
	S <sub>3</sub>	+	S <sub>4</sub>	$\rightarrow$	S <sub>7</sub>	$3 \times 10^{-17}$		Moses et al. (2002)
15	S <sub>3</sub>	+	S <sub>5</sub>	$\rightarrow$	S <sub>8</sub>	$1.11 \times 10^{-42}$	-2.00	Moses et al. (2002)
	S <sub>3</sub>	+	S <sub>5</sub>	$\rightarrow$	S <sub>8</sub>	$3 \times 10^{-17}$		Moses et al. (2002)
16	S <sub>4</sub>	+	S <sub>4</sub>	$\rightarrow$	S <sub>8</sub>	$1 \times 10^{-42}$		Mills (1998)
	S <sub>4</sub>	+	S <sub>4</sub>	$\rightarrow$	S <sub>8</sub>	$3 \times 10^{-17}$		Mills (1998)
17	S	+	O	$\rightarrow$	SO	$3.01 \times 10^{-45}$		Zhang et al. (2012)
	S	+	O	$\rightarrow$	SO	$7.27 \times 10^{-20}$	-1.00	Zhang et al. (2012)
18	S	+	SO	$\rightarrow$	S <sub>2</sub> O	$3.67 \times 10^{-43}$	-2.00	Moses et al. (2002)
	S	+	SO	$\rightarrow$	S <sub>2</sub> O	$8.86 \times 10^{-19}$	-3.00	Moses et al. (2002)
19	SO	+	HO	$\rightarrow$	HOSO	$6.45 \times 10^{-41}$	-3.48	4.90 $\times 10^2$ Goumri et al. (1999)
	SO	+	HO	$\rightarrow$	HOSO	$8.75 \times 10^{-17}$	0.50	Goumri et al. (1999)
20	SO <sub>2</sub>	+	O	$\rightarrow$	SO <sub>3</sub>	$1.32 \times 10^{-41}$		1.00 $\times 10^3$ Atkinson et al. (2004)
	SO <sub>2</sub>	+	O	$\rightarrow$	SO <sub>3</sub>	$5 \times 10^{-18}$		Atkinson et al. (2004)
21	SO <sub>2</sub>	+	H	$\rightarrow$	HSO <sub>2</sub>	$5.74 \times 10^{-43}$	-3.69	2.41 $\times 10^3$ Goumri et al. (1999)
	SO <sub>2</sub>	+	H	$\rightarrow$	HSO <sub>2</sub>	$2.31 \times 10^{-17}$	0.62	1.82 $\times 10^3$ Goumri et al. (1999)
22	SO <sub>2</sub>	+	H	$\rightarrow$	HOSO	$9.43 \times 10^{-40}$	-4.36	5.44 $\times 10^3$ Goumri et al. (1999)
	SO <sub>2</sub>	+	H	$\rightarrow$	HOSO	$9.13 \times 10^{-18}$	0.96	4.32 $\times 10^3$ Goumri et al. (1999)
23	SO	+	O	$\rightarrow$	SO <sub>2</sub>	$4.82 \times 10^{-43}$	-2.17	Lu et al. (2003)
	SO	+	O	$\rightarrow$	SO <sub>2</sub>	$3.5 \times 10^{-17}$	0.00	Lu et al. (2003)
24	SO <sub>2</sub>	+	HO	$\rightarrow$	HSO <sub>3</sub>	$3.3 \times 10^{-43}$	-4.30	Sander et al. (2006)
	SO <sub>2</sub>	+	HO	$\rightarrow$	HSO <sub>3</sub>	$1.6 \times 10^{-18}$	0.00	Sander et al. (2006)
25	HS	+	NO	$\rightarrow$	HSNO	$2.4 \times 10^{-43}$	-3.00	Demore et al. (1997)
	HS	+	NO	$\rightarrow$	HSNO	$2.71 \times 10^{-17}$		Demore et al. (1997)
26	HS	+	O <sub>2</sub>	$\rightarrow$	HSO <sub>2</sub>	$9.18 \times 10^{-46}$	-1.69	Goumri et al. (1995)
	HS	+	O <sub>2</sub>	$\rightarrow$	HSO <sub>2</sub>	$2.01 \times 10^{-16}$	0.31	Goumri et al. (1995)
27	HS	+	O <sub>2</sub>	$\rightarrow$	HSOO	$9.06 \times 10^{-46}$	-2.01	1.00 $\times 10^1$ Goumri et al. (1999)
	HS	+	O <sub>2</sub>	$\rightarrow$	HSOO	$3.3 \times 10^{-16}$	-0.26	1.50 $\times 10^2$ Goumri et al. (1999)
28	HS	+	H	$\rightarrow$	H <sub>2</sub> S	$1 \times 10^{-42}$	-2.00	Krasnopolsky (2007)
	HS	+	H	$\rightarrow$	H <sub>2</sub> S	$2.41 \times 10^{-17}$	-3.00	Krasnopolsky (2007)
29	HSO	$\rightarrow$	H	+	SO	$1.4 \times 10^{-14}$		2.95 $\times 10^4$ Tsuchiya et al. (1994)
	HSO	$\rightarrow$	H	+	SO	$3.38 \times 10^{+11}$	-1.00	2.95 $\times 10^4$ Tsuchiya et al. (1994)
30	HOSO	$\rightarrow$	HSO <sub>2</sub>			$3.18 \times 10^{-09}$	-5.64	2.79 $\times 10^4$ Goumri et al. (1999)
	HOSO	$\rightarrow$	HSO <sub>2</sub>			$3.64 \times 10^{+11}$	1.03	2.52 $\times 10^4$ Goumri et al. (1999)
31	HSOO	$\rightarrow$	O	+	HSO	$4.61 \times 10^{-10}$	-5.87	1.56 $\times 10^4$ Goumri et al. (1999)
	HSOO	$\rightarrow$	O	+	HSO	$4.53 \times 10^{+16}$	-1.07	1.43 $\times 10^4$ Goumri et al. (1999)
32	H <sub>2</sub> S <sub>2</sub>	$\rightarrow$	HS	+	HS	$3.43 \times 10^{-13}$	1.00	2.87 $\times 10^4$ Tsuchiya et al. (1994)
	H <sub>2</sub> S <sub>2</sub>	$\rightarrow$	HS	+	HS	$8.28 \times 10^{+12}$		2.87 $\times 10^4$ Tsuchiya et al. (1994)

**Table A3.** The 3-body reactions of the sulphur network used in this work.  $\alpha$ ,  $\beta$  and  $\gamma$  (K) refer to the three constants used in the arrhenius equation, such that the rate of reaction is  $k = \alpha(T/300\text{ K})^\beta \exp(-\gamma/T) \text{ m}^3\text{ s}^{-1}$ .

No.	Reaction					$\alpha$	$\beta$	$\gamma$ (K)	Reference
33	CS <sub>2</sub>	+	HO	→	CS <sub>2</sub> OH	$8 \times 10^{-43}$			<a href="#">Atkinson et al. (1992)</a>
	CS <sub>2</sub>	+	HO	→	CS <sub>2</sub> OH	$8 \times 10^{-18}$			<a href="#">Atkinson et al. (1992)</a>
34	CO	+	S	→	OCS	$3 \times 10^{-45}$		$1.00 \times 10^3$	<a href="#">Krasnopolsky (2007)</a>
	CO	+	S	→	OCS	$7.24 \times 10^{-20}$	-1.00	$1.00 \times 10^3$	<a href="#">Krasnopolsky (2007)</a>
35	CH <sub>3</sub>	+	HS	→	CH <sub>3</sub> SH	$6.88 \times 10^{-43}$	1.00		<a href="#">Shum &amp; Benson (1985)</a>
	CH <sub>3</sub>	+	HS	→	CH <sub>3</sub> SH	$1.66 \times 10^{-17}$			<a href="#">Shum &amp; Benson (1985)</a>

**Table A4.** The 2-body reactions of the sulphur network used in this work.  $\alpha$ ,  $\beta$  and  $\gamma$  (K) refer to the three constants used in the arrhenius equation, such that the rate of reaction is  $k = \alpha(T/300\text{ K})^\beta \exp(-\gamma/T) \text{ m}^3\text{ s}^{-1}$ .

No.	Reaction				$\alpha$	$\beta$	$\gamma$ (K)	Reference		
1	S	+	S <sub>3</sub>	→	S <sub>2</sub>	+	S <sub>2</sub>	$8 \times 10^{-17}$		Moses et al. (2002)
2	S	+	S <sub>4</sub>	→	S <sub>2</sub>	+	S <sub>3</sub>	$8 \times 10^{-17}$		Moses et al. (2002)
3	S	+	S <sub>5</sub>	→	S <sub>2</sub>	+	S <sub>4</sub>	$5 \times 10^{-17}$		2.00×10 <sup>2</sup> Moses et al. (2002)
4	S	+	S <sub>6</sub>	→	S <sub>2</sub>	+	S <sub>5</sub>	$5 \times 10^{-17}$		3.00×10 <sup>2</sup> Moses et al. (2002)
5	S	+	S <sub>7</sub>	→	S <sub>2</sub>	+	S <sub>6</sub>	$4 \times 10^{-17}$		2.00×10 <sup>2</sup> Moses et al. (2002)
6	S	+	S <sub>8</sub>	→	S <sub>2</sub>	+	S <sub>7</sub>	$4 \times 10^{-17}$		4.00×10 <sup>2</sup> Moses et al. (2002)
7	S	+	S <sub>5</sub>	→	S <sub>3</sub>	+	S <sub>3</sub>	$3 \times 10^{-17}$		2.00×10 <sup>2</sup> Moses et al. (2002)
8	S	+	S <sub>6</sub>	→	S <sub>3</sub>	+	S <sub>4</sub>	$3 \times 10^{-17}$		3.00×10 <sup>2</sup> Moses et al. (2002)
9	S	+	S <sub>7</sub>	→	S <sub>3</sub>	+	S <sub>5</sub>	$2 \times 10^{-17}$		2.00×10 <sup>2</sup> Moses et al. (2002)
10	S	+	S <sub>8</sub>	→	S <sub>3</sub>	+	S <sub>6</sub>	$2 \times 10^{-17}$		4.00×10 <sup>2</sup> Moses et al. (2002)
11	S	+	S <sub>7</sub>	→	S <sub>4</sub>	+	S <sub>4</sub>	$2 \times 10^{-17}$		2.00×10 <sup>2</sup> Moses et al. (2002)
12	S	+	S <sub>8</sub>	→	S <sub>4</sub>	+	S <sub>5</sub>	$2 \times 10^{-17}$		4.00×10 <sup>2</sup> Moses et al. (2002)
13	S <sub>2</sub>	+	S <sub>8</sub>	→	S <sub>5</sub>	+	S <sub>5</sub>	$1 \times 10^{-17}$		1.40×10 <sup>3</sup> Moses et al. (2002)
14	S <sub>3</sub>	+	S <sub>5</sub>	→	S <sub>2</sub>	+	S <sub>6</sub>	$4 \times 10^{-17}$		2.00×10 <sup>2</sup> Moses et al. (2002)
15	S <sub>3</sub>	+	S <sub>7</sub>	→	S <sub>2</sub>	+	S <sub>8</sub>	$3 \times 10^{-17}$		2.00×10 <sup>2</sup> Moses et al. (2002)
16	S <sub>3</sub>	+	S <sub>7</sub>	→	S <sub>4</sub>	+	S <sub>6</sub>	$1 \times 10^{-17}$		2.00×10 <sup>2</sup> Moses et al. (2002)
17	S <sub>3</sub>	+	S <sub>4</sub>	→	S <sub>2</sub>	+	S <sub>5</sub>	$4 \times 10^{-17}$		2.00×10 <sup>2</sup> Moses et al. (2002)
18	S <sub>3</sub>	+	S <sub>6</sub>	→	S <sub>2</sub>	+	S <sub>7</sub>	$4 \times 10^{-18}$		3.00×10 <sup>2</sup> Moses et al. (2002)
19	S <sub>3</sub>	+	S <sub>7</sub>	→	S <sub>5</sub>	+	S <sub>5</sub>	$1 \times 10^{-17}$		2.00×10 <sup>2</sup> Moses et al. (2002)
20	S <sub>4</sub>	+	S <sub>5</sub>	→	S <sub>2</sub>	+	S <sub>7</sub>	$2 \times 10^{-18}$		2.00×10 <sup>2</sup> Moses et al. (2002)
21	S <sub>4</sub>	+	S <sub>6</sub>	→	S <sub>2</sub>	+	S <sub>8</sub>	$2 \times 10^{-18}$		3.00×10 <sup>2</sup> Moses et al. (2002)
22	S <sub>4</sub>	+	S <sub>5</sub>	→	S <sub>3</sub>	+	S <sub>6</sub>	$2 \times 10^{-18}$		2.00×10 <sup>2</sup> Moses et al. (2002)
23	S <sub>4</sub>	+	S <sub>7</sub>	→	S <sub>3</sub>	+	S <sub>8</sub>	$5 \times 10^{-18}$		2.00×10 <sup>2</sup> Moses et al. (2002)
24	S <sub>4</sub>	+	S <sub>6</sub>	→	S <sub>5</sub>	+	S <sub>5</sub>	$2 \times 10^{-18}$		3.00×10 <sup>2</sup> Moses et al. (2002)
25	S <sub>4</sub>	+	S <sub>7</sub>	→	S <sub>5</sub>	+	S <sub>6</sub>	$5 \times 10^{-18}$		2.00×10 <sup>2</sup> Moses et al. (2002)
26	O	+	S <sub>2</sub>	→	S	+	SO	$2 \times 10^{-17}$		$8.40 \times 10^1$ Craven & Murrell (1987)
27	O	+	S <sub>3</sub>	→	S <sub>2</sub>	+	SO	$8 \times 10^{-17}$		Moses et al. (2002)
28	O	+	S <sub>4</sub>	→	S <sub>3</sub>	+	SO	$8 \times 10^{-17}$		Moses et al. (2002)
29	O	+	S <sub>5</sub>	→	S <sub>4</sub>	+	SO	$8 \times 10^{-17}$		2.00×10 <sup>2</sup> Moses et al. (2002)
30	O	+	S <sub>6</sub>	→	S <sub>5</sub>	+	SO	$8 \times 10^{-17}$		3.00×10 <sup>2</sup> Moses et al. (2002)
31	O	+	S <sub>7</sub>	→	S <sub>6</sub>	+	SO	$8 \times 10^{-17}$		2.00×10 <sup>2</sup> Moses et al. (2002)
32	O	+	S <sub>8</sub>	→	S <sub>7</sub>	+	SO	$8 \times 10^{-17}$		4.00×10 <sup>2</sup> Moses et al. (2002)
33	S	+	O <sub>2</sub>	→	SO	+	O	$2.51 \times 10^{-17}$		$1.84 \times 10^3$ Miyoshi et al. (1996)
34	S	+	SO <sub>2</sub>	→	SO	+	SO	$9.77 \times 10^{-18}$		$4.54 \times 10^3$ Isshiki et al. (2003)
35	S	+	H <sub>2</sub>	→	H	+	HS	$3.04 \times 10^{-19}$	2.70	$6.46 \times 10^3$ Shiina et al. (1996) and Woiki & Roth (1995)
36	S	+	OCS	→	CO	+	S <sub>2</sub>	$1.35 \times 10^{-19}$	2.70	$1.20 \times 10^3$ Shiina et al. (1996) and Lu et al. (2006)
37	S	+	CS <sub>2</sub>	→	CS	+	S <sub>2</sub>	$2.82 \times 10^{-16}$		$5.92 \times 10^3$ Woiki & Roth (1995)
38	S	+	C <sub>2</sub> H <sub>6</sub>	→	HS	+	C <sub>2</sub> H <sub>5</sub>	$2.04 \times 10^{-16}$		$7.42 \times 10^3$ Tsuchiya et al. (1996)
39	S	+	CH <sub>4</sub>	→	HS	+	CH <sub>3</sub>	$3.39 \times 10^{-16}$		$1.00 \times 10^4$ Tsuchiya et al. (1996)
40	S	+	HS	→	S <sub>2</sub>	+	H	$4.98 \times 10^{-18}$		Nicholas et al. (1979)
41	S	+	HO <sub>2</sub>	→	SO	+	HO	$5.84 \times 10^{-17}$		Zhang et al. (2012)
42	S	+	SO <sub>3</sub>	→	SO <sub>2</sub>	+	SO	$1 \times 10^{-22}$		Moses et al. (2002)
43	S	+	HO	→	SO	+	H	$6.6 \times 10^{-17}$		Demore et al. (1997)
44	S	+	S <sub>2</sub> O	→	S <sub>2</sub>	+	SO	$1 \times 10^{-18}$		$1.20 \times 10^3$ Moses et al. (2002)
45	S	+	O <sub>3</sub>	→	SO	+	O <sub>2</sub>	$1.2 \times 10^{-17}$		Atkinson et al. (2004)
46	S <sub>3</sub>	+	CO	→	OCS	+	S <sub>2</sub>	$1 \times 10^{-17}$		$2.00 \times 10^4$ Krasnopolsky (2007)
47	S <sub>3</sub>	+	H	→	HS	+	S <sub>2</sub>	$1.2 \times 10^{-16}$		$1.95 \times 10^3$ Krasnopolsky (2007)
48	HS	+	HS	→	H <sub>2</sub> S	+	S	$1.5 \times 10^{-17}$		Schofield (1973)
49	HS	+	HO	→	H <sub>2</sub> O	+	S	$2.5 \times 10^{-18}$		Krasnopolsky (2007)
50	HS	+	O	→	H	+	SO	$1.3 \times 10^{-16}$		Tsuchiya et al. (1994)
51	HS	+	NO <sub>2</sub>	→	NO	+	HSO	$6.49 \times 10^{-17}$		Atkinson et al. (2004)
52	HS	+	N <sub>2</sub> O	→	N <sub>2</sub>	+	HSO	$5 \times 10^{-22}$		Herndon et al. (1999)
53	HS	+	O <sub>3</sub>	→	O <sub>2</sub>	+	HSO	$1.1 \times 10^{-17}$		$2.80 \times 10^2$ Wang & Howard (1990)
54	HS	+	O <sub>2</sub>	→	O	+	HSO	$3.11 \times 10^{-17}$		$9.02 \times 10^3$ Tsuchiya et al. (1997)
55	HS	+	O <sub>2</sub>	→	HO	+	SO	$4 \times 10^{-25}$		Demore et al. (1997)
56	HS	+	CO	→	OCS	+	H	$4.15 \times 10^{-20}$		$7.66 \times 10^3$ Kurbanov & Mamedov (1995)
57	HS	+	H <sub>2</sub> CS	→	H <sub>2</sub> S	+	HCS	$8.14 \times 10^{-17}$		$3.18 \times 10^3$ Vandeputte et al. (2010)



**Table A5.** The 2-body reactions of the sulphur network used in this work.  $\alpha$ ,  $\beta$  and  $\gamma$  (K) refer to the three constants used in the arrhenius equation, such that the rate of reaction is  $k = \alpha(T/300\text{K})^\beta \exp(-\gamma/T) \text{ m}^3\text{s}^{-1}$ .

No.	Reaction						$\alpha$	$\beta$	$\gamma$ (K)	Reference	
58	H <sub>2</sub> S	+	O	→	H	+	HSO	$5 \times 10^{-16}$		$3.85 \times 10^3$	Tsuchiya et al. (1994)
59	H <sub>2</sub> S	+	O	→	HO	+	HS	$2.01 \times 10^{-16}$		$3.85 \times 10^3$	Tsuchiya et al. (1994)
60	H <sub>2</sub> S	+	H	→	H <sub>2</sub>	+	HS	$3.07 \times 10^{-18}$	2.10	$3.52 \times 10^2$	Yoshimura et al. (1992)
61	H <sub>2</sub> S	+	O <sub>2</sub>	→	HO <sub>2</sub>	+	HS	$3.1 \times 10^{-18}$	2.76	$1.92 \times 10^4$	Montoya et al. (2005)
62	H <sub>2</sub> S	+	HO	→	H <sub>2</sub> O	+	HS	$1.61 \times 10^{-17}$		$5.40 \times 10^2$	Mousavipour et al. (2003)
63	H <sub>2</sub> S	+	HO <sub>2</sub>	→	H <sub>2</sub> O	+	HSO	$5 \times 10^{-18}$			Bulatov et al. (1990)
64	H <sub>2</sub> S	+	CH <sub>3</sub>	→	CH <sub>4</sub>	+	HS	$1.05 \times 10^{-19}$	1.20	$7.22 \times 10^2$	Mousavipour et al. (2003)
65	H <sub>2</sub> S	+	SO <sub>2</sub>	→	H <sub>2</sub> O	+	S <sub>2</sub> O	$1.09 \times 10^{-19}$	1.86	$1.90 \times 10^4$	Sendt & Haynes (2005)
66	H <sub>2</sub> S	+	S <sub>2</sub> O	→	H <sub>2</sub> O	+	S <sub>3</sub>	$7.08 \times 10^{-19}$	1.51	$1.71 \times 10^4$	Sendt & Haynes (2005)
67	SO	+	HO <sub>2</sub>	→	SO <sub>2</sub>	+	HO	$2.8 \times 10^{-17}$			Zhang et al. (2012)
68	SO	+	S <sub>3</sub>	→	S <sub>2</sub> O	+	S <sub>2</sub>	$1 \times 10^{-18}$			Moses et al. (2002)
69	SO	+	O <sub>3</sub>	→	SO <sub>2</sub>	+	O <sub>2</sub>	$4.5 \times 10^{-18}$		$1.17 \times 10^3$	Atkinson et al. (2004)
70	SO	+	O <sub>3</sub>	→	SO <sub>2</sub>	+	O <sub>2</sub> (a <sup>1</sup> Δg)	$3.6 \times 10^{-19}$		$1.10 \times 10^3$	Sander et al. (2006)
71	SO	+	O <sub>2</sub>	→	SO <sub>2</sub>	+	O	$4.37 \times 10^{-20}$	1.40	$1.87 \times 10^3$	Garland (1998)
72	SO	+	CO <sub>2</sub>	→	SO <sub>2</sub>	+	CO	$1.5 \times 10^{-17}$		$2.20 \times 10^4$	Bauer et al. (1971)
73	SO	+	NO <sub>2</sub>	→	SO <sub>2</sub>	+	NO	$1.4 \times 10^{-17}$			Atkinson et al. (2004)
74	SO	+	SO <sub>3</sub>	→	SO <sub>2</sub>	+	SO <sub>2</sub>	$2 \times 10^{-21}$			Chung et al. (1975)
75	SO <sub>2</sub>	+	H	→	HO	+	SO	$4.58 \times 10^{-14}$	-2.30	$1.56 \times 10^4$	Blitz et al. (2006)
76	SO <sub>2</sub>	+	NO <sub>3</sub>	→	SO <sub>3</sub>	+	NO <sub>2</sub>	$1.8 \times 10^{-28}$			Kurten et al. (2010)
77	SO <sub>2</sub>	+	O <sub>3</sub>	→	SO <sub>3</sub>	+	O <sub>2</sub>	$3.01 \times 10^{-18}$		$7.00 \times 10^3$	Demore et al. (1997)
78	SO <sub>2</sub>	+	HO <sub>2</sub>	→	HO	+	SO <sub>3</sub>	$2.26 \times 10^{-19}$		$3.42 \times 10^3$	Hwang et al. (2010)
79	SO <sub>2</sub>	+	HO <sub>2</sub>	→	O <sub>2</sub>	+	HOSO	$8.6 \times 10^{-16}$		$5.23 \times 10^3$	Wang & Hou (2005)
80	SO <sub>2</sub>	+	O <sub>3</sub>	→	SO <sub>3</sub>	+	O <sub>2</sub> (a <sup>1</sup> Δg)	$6 \times 10^{-20}$		$7.00 \times 10^3$	Zhang et al. (2012)
81	SO <sub>2</sub>	+	O( <sup>1</sup> D)	→	SO	+	O <sub>2</sub>	$1.3 \times 10^{-16}$			Moses et al. (2002)
82	SO <sub>2</sub>	+	NO <sub>2</sub>	→	SO <sub>3</sub>	+	NO	$2 \times 10^{-32}$			Penzhorn & Canosa (1983)
83	SO <sub>3</sub>	+	O	→	SO <sub>2</sub>	+	O <sub>2</sub>	$1.06 \times 10^{-19}$	2.57	$1.47 \times 10^4$	Hindiyarti et al. (2007)
84	SO <sub>3</sub>	+	H	→	HO	+	SO <sub>2</sub>	$1.46 \times 10^{-17}$	1.22	$1.67 \times 10^3$	Hindiyarti et al. (2007)
85	SO <sub>3</sub>	+	S <sub>2</sub>	→	S <sub>2</sub> O	+	SO <sub>2</sub>	$2 \times 10^{-22}$			Moses et al. (2002)
86	SO <sub>3</sub>	+	CO	→	CO <sub>2</sub>	+	SO <sub>2</sub>	$1 \times 10^{-17}$		$1.30 \times 10^4$	Krasnopolsky VA (1994)
87	S <sub>2</sub> O	+	O	→	SO	+	SO	$1.7 \times 10^{-18}$			Mills (1998)
88	S <sub>2</sub> O	+	S <sub>2</sub> O	→	S <sub>3</sub>	+	SO <sub>2</sub>	$1 \times 10^{-20}$			Mills (1998)
89	OCS	+	O	→	CO	+	SO	$1.99 \times 10^{-17}$		$2.15 \times 10^3$	Wei & Timmons (1975)
90	OCS	+	O	→	CO <sub>2</sub>	+	S	$8.3 \times 10^{-17}$		$5.53 \times 10^3$	Singleton & Cvetanovic (1988)
91	OCS	+	C	→	CO	+	CS	$1.01 \times 10^{-16}$			Dorthe et al. (1991)
92	OCS	+	NO <sub>3</sub>	→	CO	+	SO	$1 \times 10^{-22}$			Atkinson et al. (2004)
93	OCS	+	HO	→	CO <sub>2</sub>	+	HS	$1.1 \times 10^{-19}$		$1.20 \times 10^3$	Sander et al. (2006)
94	CS	+	O	→	CO	+	S	$2.61 \times 10^{-16}$		$7.58 \times 10^2$	Lilenfeld & Richardson (1977)
95	CS	+	HO	→	H	+	OCS	$1.7 \times 10^{-16}$			Wakelam et al. (2015)
96	CS	+	HO	→	CO	+	HS	$3 \times 10^{-17}$			Wakelam et al. (2015)
97	CS	+	C	→	S	+	C <sub>2</sub>	$1.44 \times 10^{-17}$	0.5	$2.04 \times 10^4$	Wakelam et al. (2015)
98	CS	+	C <sub>2</sub> H <sub>3</sub>	→	H <sub>2</sub> C <sub>3</sub> S	+	H	$1.7 \times 10^{-18}$		$4.00 \times 10^2$	Wakelam et al. (2015)
99	CS	+	CH	→	S	+	C <sub>2</sub> H	$5 \times 10^{-17}$			Wakelam et al. (2015)
100	CS	+	HN	→	S	+	HNC	$1 \times 10^{-17}$		$1.20 \times 10^3$	Wakelam et al. (2015)
101	CS	+	NO <sub>2</sub>	→	OCS	+	NO	$7.61 \times 10^{-23}$			Black et al. (1983)
102	CS	+	O <sub>3</sub>	→	OCS	+	O <sub>2</sub>	$3.01 \times 10^{-22}$			Black et al. (1983)
103	CS	+	O <sub>2</sub>	→	OCS	+	O	$2.62 \times 10^{-22}$		$1.86 \times 10^3$	Richardson (1975)
104	CS <sub>2</sub>	+	O	→	CS	+	SO	$2.76 \times 10^{-17}$		$6.44 \times 10^2$	Wei & Timmons (1975)
105	CS <sub>2</sub>	+	O	→	CO	+	S <sub>2</sub>	$1.08 \times 10^{-19}$			Cooper & Hershberger (1992)
106	CS <sub>2</sub>	+	O	→	OCS	+	S	$3.65 \times 10^{-18}$		$5.83 \times 10^3$	Singleton & Cvetanovic (1988)
107	CS <sub>2</sub>	+	HO	→	OCS	+	HS	$1.7 \times 10^{-21}$			Atkinson et al. (2004)
108	HSO <sub>3</sub>	+	O <sub>2</sub>	→	HO <sub>2</sub>	+	SO <sub>3</sub>	$1.3 \times 10^{-18}$		$3.30 \times 10^2$	Atkinson et al. (1992)
109	HSO	+	NO <sub>2</sub>	→	NO	+	HSO <sub>2</sub>	$9.6 \times 10^{-18}$			Demore et al. (1997)
110	HSO	+	O <sub>3</sub>	→	O <sub>2</sub>	+	O <sub>2</sub>	$2.54 \times 10^{-19}$		$3.84 \times 10^2$	Wang & Howard (1990)
111	HSO <sub>2</sub>	+	O <sub>2</sub>	→	HO <sub>2</sub>	+	SO <sub>2</sub>	$3.01 \times 10^{-19}$			Demore et al. (1997)
112	HSOO	+	O <sub>2</sub>	→	HO <sub>2</sub>	+	SO <sub>2</sub>	$3.01 \times 10^{-19}$			Demore et al. (1997)
113	H <sub>2</sub> CS	+	H	→	H <sub>2</sub>	+	HCS	$9.33 \times 10^{-17}$		$3.57 \times 10^3$	Vandeputte et al. (2010)
114	H <sub>2</sub> CS	+	CH <sub>3</sub>	→	CH <sub>4</sub>	+	HCS	$2.57 \times 10^{-17}$		$4.93 \times 10^3$	Vandeputte et al. (2010)
115	CH <sub>3</sub> SH	+	H	→	CH <sub>3</sub>	+	H <sub>2</sub> S	$1.15 \times 10^{-17}$		$8.41 \times 10^2$	Amano et al. (1983)